2008

Effects of Zn doping and high energy ball milling on the photocatalytic properties of TiO2

Paula C. Algarin
University of South Florida

Effects of Zn Doping and High Energy Ball Milling on the Photocatalytic Properties of TiO_2

by

Paula C. Algarín

A thesis submitted in partial fulfillment
of the requirements for the degree of
Master of Science in Electrical Engineering
Department of Electrical Engineering
College of Engineering
University of South Florida

Major Professor: E.K. Stefanakos, Ph.D.
D. Yogi Goswami, Ph.D.
Nikolai Kislov, Ph.D.

Date of Approval
March 26,, 2008

Keywords: photocatalysis, methyl orange, surface, band gap, sol-gel process

DEDICATION

I dedicate this thesis to my husband, for his love and support in every step of this long way, for a brand new beginning. I hope to honor him, for every night I thought I could not do it and he held me tight and told me I could.

I want to share this work with my mother and my family back home, for their love and support that always keep me going.

ACKNOWLEDGEMENTS

I would like to thank my advisor, Dr. Elias Stefanakos, for the opportunity to work with him and the members of the Clean Energy Research Center. I would like to thank Matt Smith, I greatly appreciate the trust and confidence he placed in me in that first interview when I first came to this country. I would also like to especially thank Dr. Nikolai Kislov for his wisdom, guidance, patience and enthusiasm; Dr Sesha Srinivasan for all his help, guidance and for teaching me during this process. Their help will never be forgotten and always be remembered. I would also like to thank Dr. Yogi Goswami for his guidance and insights.

I would also like to thank the staff and faculty of CERC. I would especially like to recognize the guidance and assistance given to me by Dr. Nikhil Kothurkar and Mr. Chuck Garretson. I would like to thank the staff of NNRC for the assistance and support during this work, especially Dr. Yusuf Emirov. Last but not least, I would like to thank all my fellow students associated with CERC for their help and support with my project, especially Mr. Mark Schmidt.

NOTE TO READER

The original of this document contains color that is necessary for understanding the data. The original thesis is on file with the USF library in Tampa, Florida.

TABLE OF CONTENTS

LIST OF TABLES

LIST OF FIGURES

EFFECTS OF ZN DOPING AND HIGH ENERGY BALL MILLING ON THE PHOTOCATALYTIC PROPERTIES OF TIO_2

Paula C. Algarín

ABSTRACT

TiO_2 photocatalysis is been widely studied for air and water purification applications; titanium dioxide is the most used semiconductor principally because its low cost, stability and chemical properties. However it only utilizes the UV portion of the solar spectrum as an energy source (less than 4% of the total sunlight energy). This behavior is due to its high band gap value of 3.2 eV. The modification of light harvesting properties of TiO_2 by doping has become an important research topic to achieve an efficient operating range under UV and visible light. In addition, the structure and surface properties of photocatalysts play an important role.

This thesis explores the effects of Zn doped TiO_2, prepared by the sol-gel method, on its photocatalytic activity to decompose organics and the characterization of the doped samples. Since this study is part of a collaborative initiative, the samples were synthesized and provided by Dr. A. R. Phani from the

Department of Physics, University of L'Aquila. Preliminary examination revealed a relatively low photocatalytic efficiency of the samples. The objective is to modify/improve its properties by high energy ball milling which is expected to generate accumulations of defects, particle size reduction and an increase in the active surface area.

The characterization of doped and mechanochemically treated materials will be analyzed by optical diffuse reflectance measurements and optical absorption calculations using the Kubelka-Munk approach. The phase structure and particle size of the materials will be determined using X-ray diffraction (XRD). The BET surface area of the samples will be obtained using an Autosorb instrument. The photocatalytic properties will be studied by the analysis of decomposition of Methyl Orange in an aqueous solution. An aqueous photocatalytic tubular reactor with capability of operation using UV and/or fluorescent light will be designed and built.

CHAPTER 1: INTRODUCTION

Water pollution is one of the main problems affecting the environment due to waste products generated by industries and households. Detoxification and purification of water, to achieve drinking water quality for human use, has become the main focus of today's scientific research. The main causes of surface and groundwater contamination are the industrial effluents (even in small amounts), excessive use of pesticides, fertilizers (agrochemicals) and domestic waste landfills. The pollution is caused mainly by non-degradable organic pollutants that are not treatable by conventional techniques due to their high chemical stability and/or low biodegradability [1].

Today, one of the greatest health threats to humans is the lack of potable water because without it life on Earth would be non-existent. This has lead to research on methods to disinfect polluted water at low cost by using cheap sources of energy, i.e. the sun. Solar photochemical processes have been proposed over the years and are currently being employed to destroy toxins in water by decomposing organic pollutants using sun light and semiconductors.

Solar photochemical technology can be defined as the technology that efficiently collects solar photons and uses them to promote specific chemical reactions [2]. In other words, this technology will allow us to take advantage of

the energy from the sun by means of a photochemical process called photocatalysis [1].

The titanium dioxide (TiO_2) photocatalyst is being widely studied for air and water purification applications and has emerged as an excellent photocatalytic material for environmental purification because of its high stability, low cost, non toxicity, high oxidation potential and chemically favorable properties. [3]. However it only utilizes the UV portion of the solar spectrum as an energy source (less than 4% of the total sunlight energy). This behavior is due to its high band gap value of 3.2 eV. The modification of light harvesting properties of TiO_2 by doping has become an important research topic to achieve an efficient operation range under UV and visible light. In addition, structural and surface properties of photocatalysts play an important role.

This thesis explores the effects of Zn doped TiO_2 by prepared by the sol-gel method on its photocatalytic activity to decompose organics and the characterization of the doped samples. The objective is to modify/improve their properties by high energy ball milling which is expected to generate accumulations of defects, particle size reduction and an increase in the active surface area.

CHAPTER 2: TITANIUM DIOXIDE

Titanium dioxide (TiO_2) is a wide-band gap semiconductor used in solar and chemical processes that has emerged as an excellent material for environmental purification [3, 4]. Titanium dioxide is an n-type semiconductor with electrons as the majority carriers and exists in three different polymorphic phases: anatase, rutile, and brookite. Anatase and rutile are the most common polymorphs that crystallize in a tetragonal lattice and their structure is described in chains of TiO_6 octahedra with different physical and chemical behavior [5, 6].

TiO_2 is non-toxic, chemically stable and low cost material that has a positive impact on the environment [4]. It has attracted more attention in environmental studies and applications due to its applicability to the treatment of pollutants and waste using photocatalysis. The term photocatalysis can be explained simply as a reaction where “light and a substance (the catalyst, in this case TiO_2) are necessary entities to influence a reaction” [7]. This definition will be explained further in the next chapter.

When TiO_2 is irradiated with light (photons), the chemical result can be applied to chemical processes to create or degrade specific compounds [4]. Investigations have concluded that the anatase particles with a large surface area are very efficient for the decomposition of pollutants in air and water [8].

2.1 Titanium Dioxide Lattice Structure

TiO_2 occurs in nature in three forms, has a stable phase called rutile and two metastable phases called anatase and brookite. Only anatase and rutile have characteristics that can be used as photocatalysts. The lattice structure for anatase and rutile is described in terms of distorted TiO_6 octahedra, this configuration consists of Ti^{4+} ions surrounded by six O^{2-} ions [5, 6], and in both structures, each titanium ion is at the centre of an oxygen octahedron and each of the oxygen has three coplanar near neighbour titanium cations.

In rutile, the oxygen ions form a slightly distorted hexagonal compact lattice; the three Ti-O-Ti angles are roughly equal to 120°. In anatase, the oxygen forms a fcc lattice and one Ti-O-Ti angle is about 180° while the two others are close to 90° [9], both structures are shown in Fig. 1.

According to band theory, semiconductors are characterized by two energetic bands: the valence band, VB, completely filled with electrons and a conduction band, CB, with higher energy and no electrons. The energetic distance between them (0.7-3.5 eV) is called the band gap and determines electronic and electric properties of the solid [10]. The band gap of anatase is 3.2 eV whereas the band gap of rutile is 3.0 eV. The difference in the bandgap value for these two phases is explained by small structural differences which affect electronic band properties [10]. Despite the higher energy required for electron-hole pair creation, anatase is reported to be more active than rutile for solar applications [6].

Band gap values also determine the color of the semiconductor, because they absorb light having energy equal to or higher than the band energy. The energy of visible light lies in the region of 1.5 (red) - 3.0 eV (violet). Thus, the semiconductors having a narrow band gap of about 1.5 eV are black, those having a band gap of about 3.0 eV are white [10].

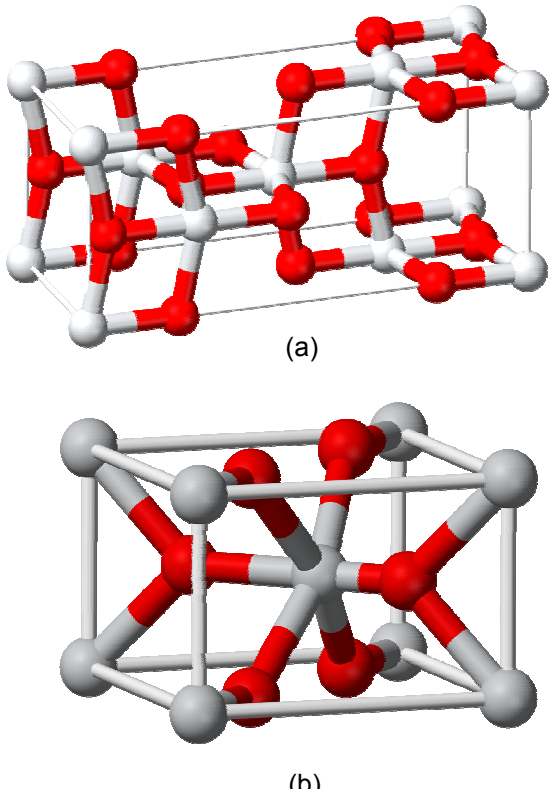

Figure 1. Stick and Ball Model Structures of TiO_2 (a) Anatase (b) Rutile. [Red balls are oxygen atoms and white balls are titanium].

2.2 TiO_2 Applications

Titanium dioxide (TiO_2) is a multifaceted compound that has a high number of industrial applications. TiO_2 is also a potent photocatalyst that can break down almost any organic compound when exposed to sunlight, and a wide

range of environmentally beneficial products are being designed such as self-cleaning fabrics, auto body finishes, and ceramic tiles. It remains to be seen, however, whether the formation of undesirable intermediate products during these processes outweigh the benefits offered by TiO_2's photocatalytic properties [4].

TiO_2 is used in the production of hydrogen and electric energy, as a gas sensor, as white pigment (e.g. in paints and cosmetic products), for corrosion-protective coatings, as an optical coating, in ceramics, and in electric devices such as varistors. Because of its non-toxicity, it plays a role in the biocompatibility of bone implants and is being discussed as a gate insulator for the new generation of MOSFETS [11]

By far, the most actively pursued applied research on TiO_2 is its use for photo-assisted degradation of organics. TiO_2 is a semiconductor and the electron–hole pairs that are created upon irradiation with sunlight can separate and the resulting charge carriers migrate to the surface where they react with adsorbed water and oxygen to produce radical species. These can attack any adsorbed organic molecules and, ultimately, lead to the complete decomposition into CO_2 and H_2O [11].

Applications of TiO_2 range from purification of wastewater (e.g. in operating rooms in hospitals) [12]; in the use of self-cleaning coatings on car windshields [13], to protect coatings of marble (preservation of ancient Greek

statues against environmental damage). Research is been done and future applications for TiO_2 are growing exponentially.

2.3 Degussa P-25 TiO_2

Degussa P-25 is generally considered the most photoactive commercially available form of TiO_2 structure which contains both separately, anatase and rutile phases in a ratio of about 3:1. P-25 is usually 20-25% rutile phase and 75-80% anatase. The average sizes of the anatase and rutile particles are 25nm and 85 nm, respectively [8]. Degussa P-25 has a surface area of approximately 50 m^2/g with anatase particles having a larger surface area than rutile particles.

Ohno et al. concluded that the larger surface area of anatase particles “improves the efficiency of decomposition of the pollutant in air and water”. Bickley et al. concluded that the increased photocatalytic activity was, in part, due to this anatase-rutile particle configuration. Anatase phase and rutile phase particles exist completely separate from one another [8, 14]; a well developed crystallinity is responsible for the high efficiency because of the low density of recombination centers, which will be explored in the following chapters [14].

CHAPTER 3: TiO_2 PHOTOCATALYSIS

3.1 Photocatalysis

A catalyst can be defined as a substance that facilitates an increase in the rate of reaction of a chemical process, which otherwise is thermodynamically favored but kinetically slow, maintaining the catalyst unaltered after the reaction. The process can be described as:

$$A \rightarrow B \qquad (1)$$

$$A + \text{Catalyst} \rightarrow B + \text{Catalyst} \qquad (2)$$

where A and B represent the reactants and products respectively.

The term photocatalysis is used when photons are involved as the mechanism to accelerate the catalyst reaction, combining the concepts of photochemistry and catalysis. Photocatalysis can be defined as a reaction where a substance (the catalyst) and a source of light (sun or an artificial light) are needed to influence a response in a reactant where the chemical structures of the reactants are modified and the catalyst remains unaltered [7] The process can be described as:

$$A + h\nu + \text{Catalyst} \rightarrow B + \text{Catalyst} \qquad (3)$$

where $h\nu$ is a quantum of energy from the incident photons that cause the reaction.

In recent years, applications to environmental clean up have been one of the most active areas in heterogeneous photocatalysis. It has become a potential technology for the treatment of organic pollutants in water such as aromatic compounds products of industrial waste that present a potential hazard to the environment and can not be treatrd by conventional techniques [15].

3.2 Basic Concepts of a Semiconductor

3.2.1 Band Gap

Semiconductors are solids whose electrical conductivity is determined by the amount of energy that is required to move electrons from the valence band to the conduction band, whereas metals have a “sea of electrons” available for conduction and insulators have no electrons. The conduction band is separated from the valence band by the defined energy gap E_g. The energy gap E_g generally refers to the energy difference between the top of the valence band and the bottom of the conduction band as shown in Figure 2 [16].

The energy gap varies from 0.7-3.5 eV and determines the electronic properties of the solid such as conductivity. When there is light absorption with sufficient energy, an electron is transferred from the valence band to the conduction band. The energy of visible light varies from 1.5 eV (red) to 3.0 eV

(violet), and can define the color of the material; a band gap of 1.5 eV is black and 3.0 eV is white [10].

In a heterogeneous photocatalysis system, after the initial excitation takes place, the generated electron-hole pairs lead to chemical reactions and molecular transformations that take place at the surface of a catalyst. The term heterogeneous photocatalysis is used to describe the charge transfer to the adsorbed species if the semiconductor catalyst remains intact during a continuous exothermic process [16].

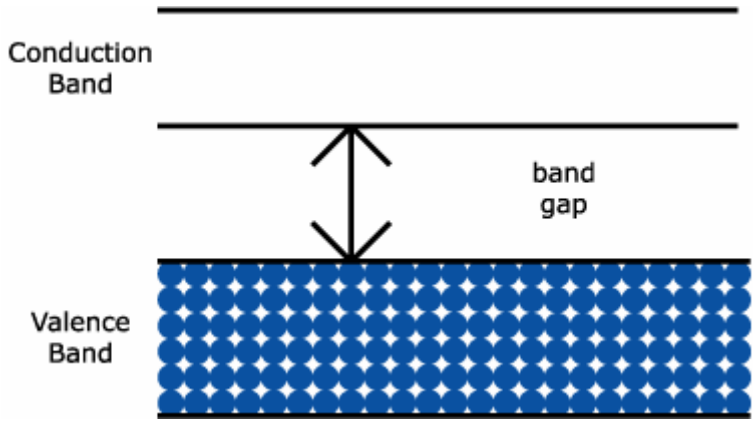

Figure 2 Semiconductor Band Gap Structure [48]

3.2.1 Electron Hole Pair, Trapping and Recombination

The most important process of photocatalysis is the photo-induced charge separation. Absorption of a photon with an energy $h\nu$ greater than or equal to the bandgap energy Eg (eV) excites an electron from the valence band to the conduction band, leading to the formation in the semiconductor of an electron/hole pair as shown in Figure. 3 [17].

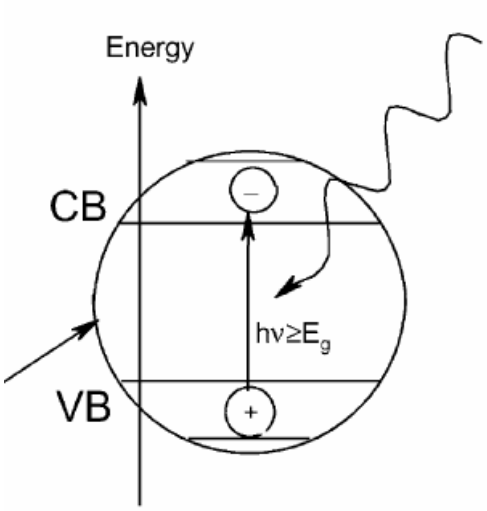

Figure 3 Electron-hole Generation [4]

For photocatalytic processes to occur, these photogenerated electrons and holes must migrate to the surface of the catalyst where they can be transferred to the adsorbed organic or inorganic pollutants. However, migration to the surface is not the only pathway the electron-hole pairs can follow as shown in Fig. 4. Once excitation occurs across the band gap the life time of the electron-hole pair is on the order of nanoseconds, which is sufficient time for them to undergo charge transfer to adsorbed species (organic or inorganic pollutants) on the semiconductor surface [16-18].

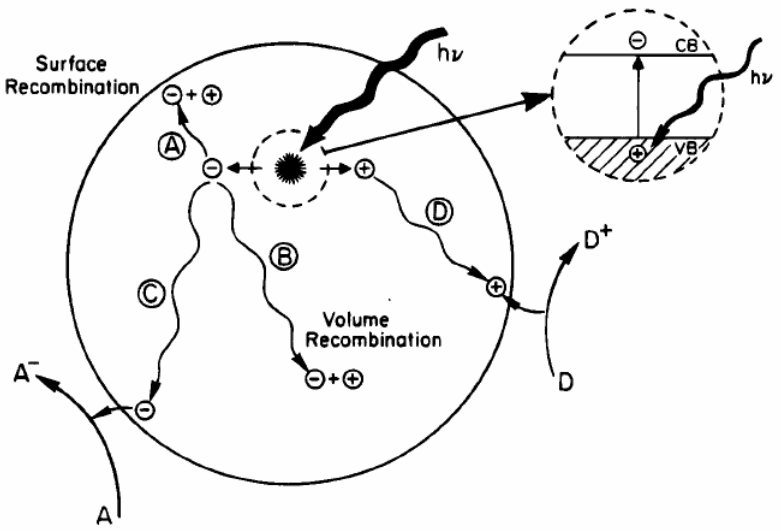

Figure 4 Schematic Photoexcitation in a Solid followed by Deexcitation Events [16].

Both surface and volume recombination can also occur, as denoted by pathways A and B. If the electron-hole recombination rate is too high it can degrade or even halt photocatalysis [16]. The concept of charge separation, by any number of means, is an important idea as it relates to doped semiconductor catalysts, and is explored further in this study. While at the surface, the semiconductor can donate electrons to reduce an electron acceptor (usually oxygen in an aerated solution, pathway C); also a hole can migrate to the surface where an electron from a donor species can combine with the surface hole oxidizing the donor species (pathway D) [16].

The efficiency of the photocatalyst in degrading the pollutant is based on different factors such as the diffusion of the electron-hole pair in the surface and, as a quantum yield, the number of events occurring per photon absorbed. In an ideal case the diffusion of the products into the solution occurs quickly without

the reverse reaction of electrons recombining with donors and holes recombining with acceptors. However, in a real system recombination does occur and the concentration of both holes and electrons is not equal. Charge separation or charge trapping is used to increase the photocatalytic effect and maintain an efficient process [16].

Since the crystal structure of the photocatalyst is not pure, but instead has both surface and bulk defects, it is expected that surface states (or charges) exist across the surface. These surface states, which differ in energy from the bulk, serve as charge carrier traps. The carrier lifetimes of the electrons and holes are therefore increased since these traps stop the recombination of electrons and holes as shown in Figure 5 [16].

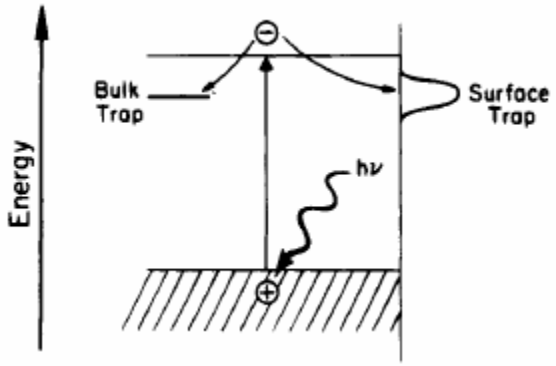

Figure 5 Surface and Bulk Electron Carrier Trapping [16].

Modifications to semiconductor surfaces such as addition of metals, dopants, or combinations with other semiconductors are beneficial in decreasing the electron-hole recombination rate and thereby increasing the quantum yield of the photocatalytic process [16].

3.3 TiO_2 in Photocatalysis

Photocatalytic reactions on TiO_2 powders have attracted much attention because of their applicability to the treatment of a variety of organic (dyes, phenols, etc.) and biological pollutants (viruses, bacteria, fungi, algae, and cancer cells), which can be totally degraded to CO_2, H_2O, and other harmless inorganic anions, eliminating their toxicity [21]. Whenever different semiconductor materials have been tested under comparable conditions for the degradation of the same compounds, TiO_2 has generally been demonstrated to be the most active [20].

When a photon is absorbed and produces energy greater than the band gap then an electron/hole pair is formed and creates an active surface site where the valence band holes can oxidize an organic compound to CO_2, H_2O and mineral acid [19]. When in contact with water, hydroxyl radicals (OH) are created and help retarding the recombination of the electron hole pairs.

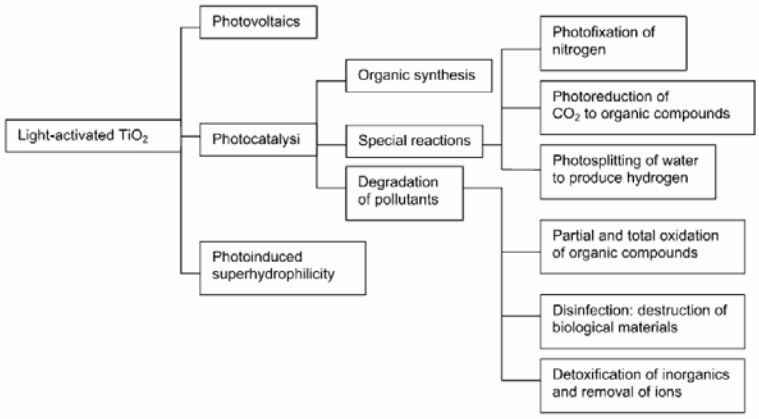

Figure 6 Photoinduced Processes in TiO_2 [4]

The photoelectrochemical properties of different structures of TiO_2, rutile and anatase, have been reported [22, 23]. The anatase form appears to be the most photoactive and the most practical for environmental applications [24]. The band gap of the anatase is 3.2 eV and is larger than the rutile band gap.

The photocatalytic activity of TiO_2 is influenced by many factors such as the preparation method, particle size, crystal microstructure, specific surface area, porosity and so on. In order to obtain a TiO_2 powder with highly photocatalytic activity for a practical purification system, these factors must be taken into consideration.

3.4 Modification to TiO_2

As mentioned previously, modifications of semiconductor surfaces by the addition of metals, dopants, or combinations with other semiconductors can play an important role in science and technology. The modified materials with their unique optical, electrical, magnetic, catalytic, and chemical properties are widely used in fields such as photoluminescence, photocatalysis, and nanoelectronics [25]. Particularly, people have tried to improve the photocatalytic activity of TiO_2 through a number of modification methods, such as noble metal doping, composite semiconductors and transition metal doping.

Many researches have focused in enhancing the photocatalytic activity of TiO_2 in the whole spectrum. Among the most widely used modification methods, transition metal doping has aroused great interest since this method can

enhance the activities of a TiO_2 photocatalyst in many types of photocatalytic reactions [26]. Another reason for the surface modification of TiO_2 is to inhibit recombination of photogenerated electrons and holes by increasing the charge separation and therefore enhancing the efficiency of the photocatalytic process. Zhao et. al. found that the photodegradation activity can be enhanced by doping by an appropriate amount of Zn which enhances the electron injection into the conduction band of TiO_2 by capturing electrons and promoting the formation of reactive oxygen species. Hence, the enhanced photodegradation of dyes under visible irradiation can be realized [32].

The modification of TiO_2 by doping with metal ions and coupling with other semiconductors can significantly influence the process of photodegradation. Marci et. al. [33] found that Zn can considerably enhance the photocatalytic performance of TiO_2 under UV irradiation, due to an increase in the separation rate of photoinduced charges because of the difference in the energy band position. The dynamic processes of photoinduced charges are affected by oxygen vacancies, and can be determined by the metal ions present on the surface of TiO_2 nanoparticles.

For this study, TiO_2 has been modified by Zn doping to improve the visible-light absorption, prevent or delay charge carrier recombination and improve its surface properties.

CHAPTER 4: EXPERIMENTAL METHODS AND PROCEDURES

4.1 XRD: X-ray Diffractometer

X-ray Powder Diffraction (XRD) is an efficient analytical technique used to characterize and identify unknown crystalline materials. The most widespread use of XRD is the identification of compounds by their diffraction pattern [34]. Monochromatic x-rays, electromagnetic radiation similar to light, but with a much shorter wavelength is used to determine the interplanar spacing of the unknown materials.

X-rays are produced when electrically charged particles of sufficient energy are deccelerated; these charges are electrons that are formed when the filament of a cathode ray tube is heated. These electrons are accelerated by means of a high voltage that draws them to a metal target. The points of impact of the electrons (anode), produce the X-rays that are radiated in all directions. Figure 7 shows the X-ray tube component mentioned earlier [35].

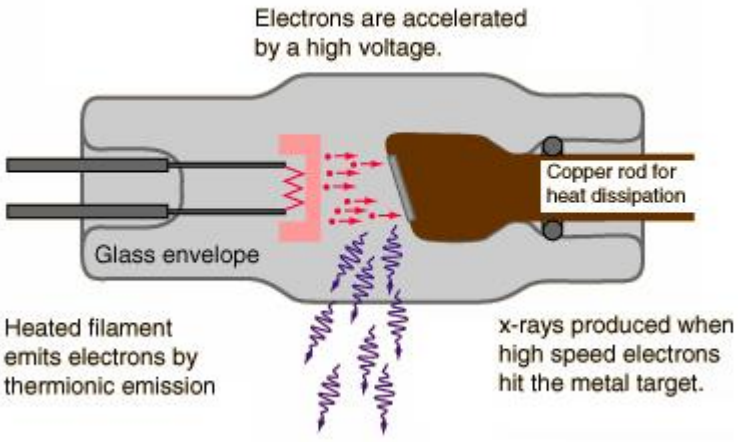

Figure 7 X-ray Tube Components [35]

For XRD analysis the X-ray beam interacts with the planes of atoms of the sample; part of the beam is transmitted, part is absorbed by the sample, part is refracted and scattered, and part is diffracted. Diffraction of an X-ray beam by a crystalline solid is analogous to diffraction of light by droplets of water, producing the familiar rainbow. X-rays are diffracted by each mineral differently, depending on what atoms make up the crystal [34]

With this technique the samples are analyzed as powders with grains in random orientations to insure that all crystallographic directions are "sampled" by the beam. The basic principle of operation of the XRD spectrometer is based on Bragg's law. When the Bragg conditions for constructive interference are obtained, a "reflection" is produced, and the relative peak height is generally proportional to the number of grains in a preferred orientation.

According to Bragg's law, to obtain constructive interference the path difference between the incident and the scattered waves, which is 2.d.sinθ, has to be a multiple of the wavelength λ. For this case, the Bragg law gives the relation between interplanar distance d and diffraction angle θ [34]:

$$2.d.\sin\theta = n.\lambda \qquad (4)$$

Where n is an integer, λ is the wavelength of X-rays, d is the spacing between the planes in the atomic lattice, and θ is the angle between the incident ray and the scattering planes; Since λ is known, θ can be measured, the d-spacing can be calculated using the Bragg's equation. Figure 8 shows the basic principles of constructive interference of the scattered X-rays.

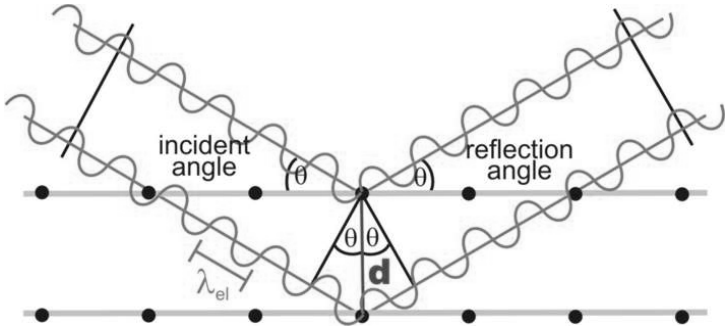

Figure 8 Constructive Interference of Reflected Waves [34]

The basic geometry of an X-ray diffractometer is shown in Figure.9; it has a source of monochromatic radiation and an X-ray detector situated on the circumference of a graduated circle centered on the powder specimen. The detector and specimen holder are mechanically coupled with a goniometer so that a rotation of the detector through 2θ degrees occurs in conjunction with the rotation of the specimen through θ degrees, a fixed 2:1 ratio. Divergent slits,

located between the X-ray source and the specimen, and between the specimen and the detector, limit scattered (non-diffracted) radiation, reduce background noise, and collimate the radiation.

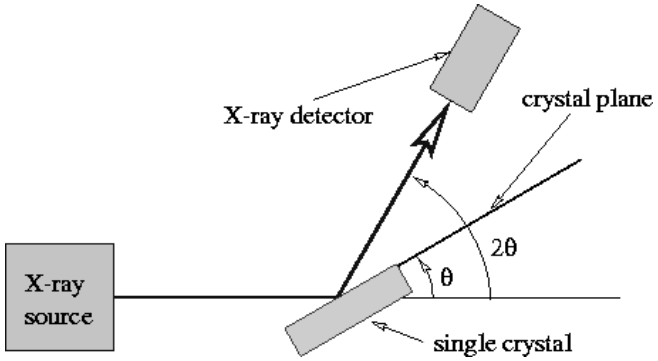

Figure 9 Basic Geometry of an X-ray Diffractometer [34]

The phase structure of the TiO_2 samples was characterized by X-ray diffraction (XRD). A Philips X'pert pro PreFix powder X-ray diffractomerter with CuKα radiation (λ=1.54060 Å) was employed for this purpose. The incident and diffraction slit width used for all the experiments are 1° and 2°, respectively, and the incident beam mask used corresponds to 10 mm. The sample preparations for the XRD measurement are strictly followed to obtain maximum signal to noise ratio.

4.2 BET Surface Area and Pore Size Distribution

Catalysts and photocatalysts are often characterized by their interaction with gases. The tendency of all solid surfaces to attract surrounding gas molecules gives rise to a process called gas sorption. Monitoring the gas sorption process provides a wealth of useful information about the characteristics of solids

such as surface area and pore size. At low temperatures, non-reactive gases (nitrogen, argon, krypton, etc.) are physisorbed by the surface. Through gas physisorption the total surface area of the sample can be calculated by the BET method [36].

Before performing a surface area analysis or pore size measurement, solid surfaces must be freed from contaminants such as water and oils. The process is call outgassing and is carried out by placing a sample in a glass cell and heating it under vacuum, or a flow of dry, inert gas. Once clean, the sample is brought to a constant temperature by means of an external bath, typically a Dewar flask containing a cryogen like liquid nitrogen. Then, small amounts of a gas (the absorbate) are admitted in steps into the evacuated sample chamber [36].

Absorbate molecules quickly find their way to the surface of every pore in the solid (the adsorbent). These molecules can either bounce off or stick to the surface. Gas molecules that stick to the surface are said to be adsorbed. The strength with which adsorbed molecules interact with the surface determines if the adsorption process is to be considered physical (weak) or chemical (strong).

In the present study, Autosorb-1C from Quantachrome Instruments has been employed to determine the surface area and pore size distribution of the samples. Each of them was placed in a glass tube and was outgassed at 300° C for 3 hours. The external bath for the sample was liquid nitrogen (77 K) and a

multi point BET method using nitrogen as the adsorbate gas was used to analyze these samples [36].

4.3 SEM: Scanning Electron Microscope

The Scanning Electron Microscope (SEM) is a type of microscope capable of producing high resolution images of a sample surface using electrons rather than light to form an image. Electron microscopy takes advantage of the wave nature of rapidly moving electrons. Where visible light has wavelengths from 4,000 to 7,000 Angstroms, electrons accelerated to 10,000 KeV have wavelengths of 0.12 Angstroms. Optical microscopes have their resolution limited by the diffraction of light to about 1000 diameters magnification. The Hitachi S800 scanning electron microscope, in the present study, is limited to magnifications of around 3,000,000 [34].

The SEM uses secondary electrons when a focused electron beam is incident on the specimen to form the image. The secondary electron signal provides information about the surface of a specimen. Since secondary electrons do not diffuse much inside the specimen, they are most suitable for observing fine structure of the specimen surface. Figure 10 shows the signals generated in an electron beam and specimen interaction.

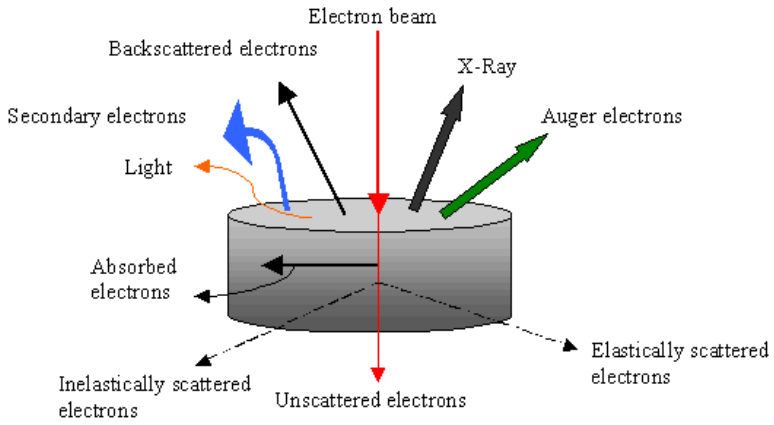

Figure 10 Electron Beam and Specimen Interaction Signals [37]

The basic diagram of the operation of the Hitachi S800 SEM is shown in Figure 11. Electrons from a filament in an electron gun are beamed at the specimen inside a vacuum chamber. The beam is collimated by electromagnetic condenser lenses, focused by an objective lens and then swept across the specimen at high speed. The secondary electrons are detected by a scintillation material that produces flashes of light from the electrons. The light flashes are then detected and amplified by a photomultiplier tube.

The microstructures of the samples in the different stages were observed by Hitachi S800 scanning electron microscope (SEM) and local phase composition was determined in the energy dispersive X-ray spectrometry (EDS) mode using the same instrument. A fixed voltage of 25 KV and resolution of 1100X and 20000X were used. Genesis software was used to analyze the SEM images and EDS mappings.

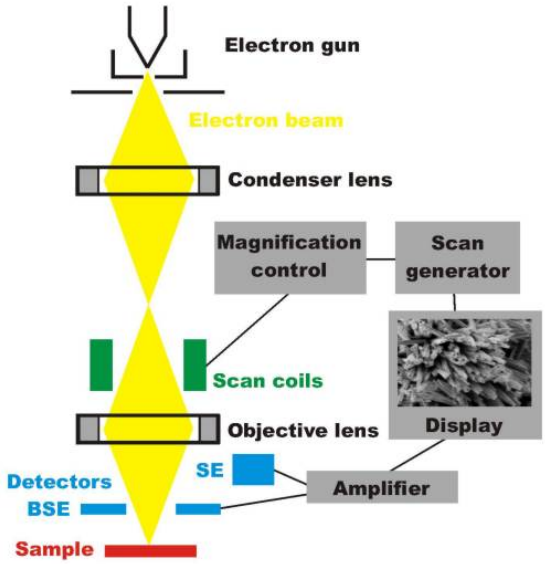

Figure 11. Schematic Working Principle Diagram for a SEM [38]

4.4 Energy Dispersive X-ray Spectroscopy (EDS)

Another important signal that can be analyzed by the Hitachi S800 SEM, when the electron beam- specimen interaction occurs is the x-ray emission. EDS identifies the elemental composition of materials imaged in a Scanning Electron Microscope (SEM) for all elements with an atomic number greater than boron (B). Most elements are detected at concentrations of the order of 0.1% excluding hydrogen. When the electron beam of the SEM hits the sample surface, it generates x-ray fluorescence from the atoms in its path. The energy of each x-ray photon is characteristic of the element which produced it. The EDS microanalysis system collects the x-rays, sorts and plots them by energy, and automatically identifies and labels the elements responsible for the peaks in this energy distribution. The liquid nitrogen cooled detector is used to capture and map the x-ray counts continuously [34].

4.5 Optical Absorption

The optical absorption data was deduced from the Kubelka–Munk function. The Kubelka Munk method is a diffuse reflectance technique that uses a salt, NaCl in this case, mixed with the powder being measured. This technique accounts for the difference in transmission and reflectance measurements due to absorption of certain wavelengths by powders. The material was diluted to about 1% by weight in NaCl and ground using a mortar and pestle. Transmission measurements were made of the powders, which were lightly packed into small sample holders, using a spectrometer. A Kubelka-Munk conversion was applied to a diffuse reflectance spectrum to compensate for any differences. Figure 12 shows the basic concept of the technique. The Kubelka-Munk equation is:

$$f(R) = \frac{(1-R)^2}{2R} = \frac{k}{s} \quad , \qquad (5)$$

where R is the absolute diffuse reflectance of the sampled layer, k is the molar absorption coefficient, and s is the scattering coefficient [6].

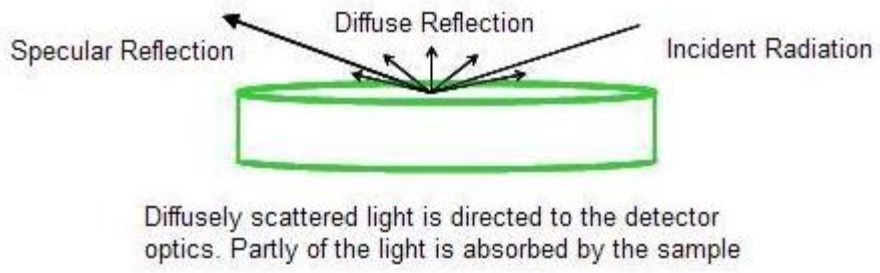

Figure 12 Kubelka-Munk Theory Basics

A linear relationship is created between the spectral intensity and the sample concentration. This equation assumes that the diluting salt is non-absorbing, that the scattering coefficient of the salt is constant, and that the sample thickness is infinite. These assumptions can be made for samples greater than 1 millimeter of highly diluted small particles. Given that we used nanoparticles and had a sample thickness of 3mm, our packing technique was the only variable that could affect the scattering coefficient.

The optical band gap, E_g, of the material can be calculated on the basis of the optical spectral absorption using the well-known formula,

$$k = \frac{A(h\upsilon - E_g)^m}{h\upsilon} \qquad (6)$$

where A is a constant, $h\nu$ is the incident photon energy, and *m* depends on the nature of band transition, *m* = ½ for direct and *m* = 2 for indirect allowed transitions. Taking into account Equation. 6, for the purpose of determining the bandgap, extrapolating the $f(R_d)^2$ and $f(R_d)^{1/2}$ versus energy curve to $f(R_d)^2 = 0$ is equivalent to carrying out the same procedure with the k^2 and $k^{1/2}$, respectively.

4.6 Photocatalytic Reactor

The photocatalytic experiments were performed using a tubular reactor that was fabricated by Mr. Chuck Garretson, who is the CERC's Project Coordinator. Figures 13 and 14 show the general configuration of the system. A one liter Pyrex beaker is used to hold the solution that was mixed by a magnetic

stirrer that also suspended the photocatalytic particles. The solution flow through the reactor casing was pumped by a peristaltic system. An aerating stone was used to diffuse either compressed air or oxygen into the suspension. Experiments were conducted using breathing quality compressed air, which was metered through gas specific flow meters.

Six UV lamps or Fluorescence lights were mounted in the reactor casing. The lights used were RPR 3500 UV fluorescent lamps that emit a gaussian distribution of light from λ 300 to 400 nm with λ_{max} = 350 nm with a nominal power of 14W and 1.5W of UV Radiation. A thermocouple, also mounted through the top plate, monitored the temperature of the solution.

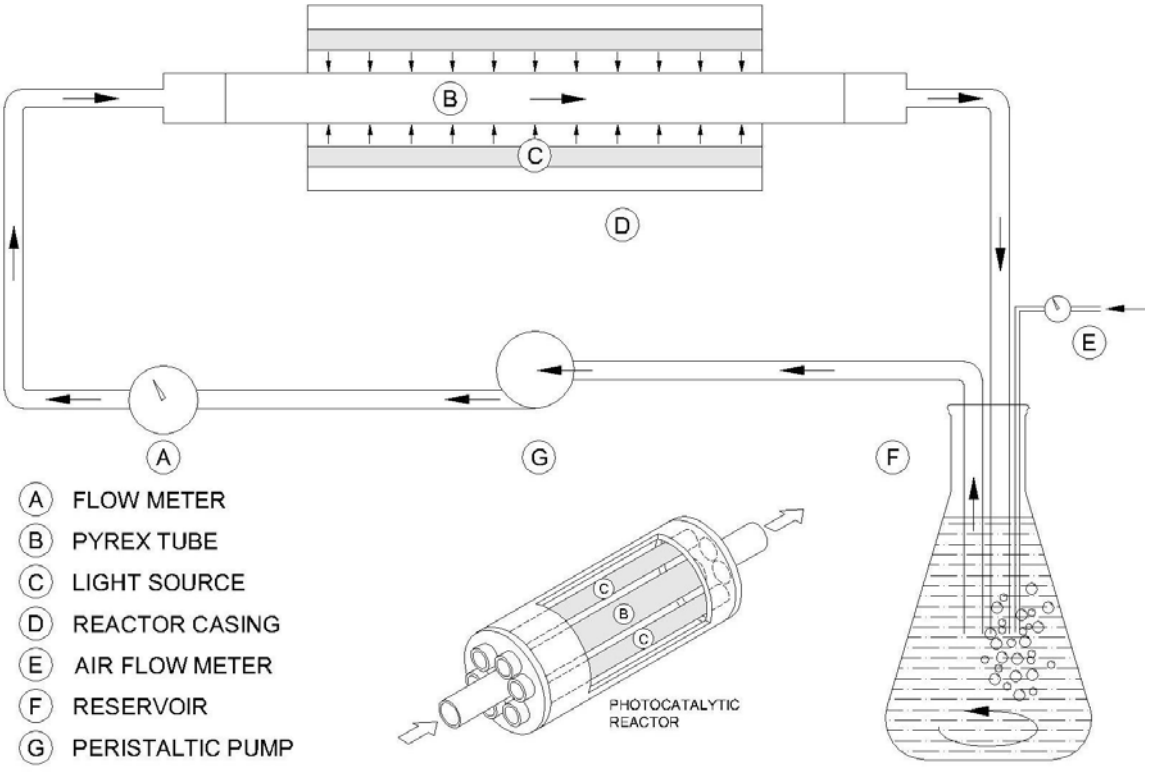

Figure 13 Tubular Reactor for Photocatalytic Experiments

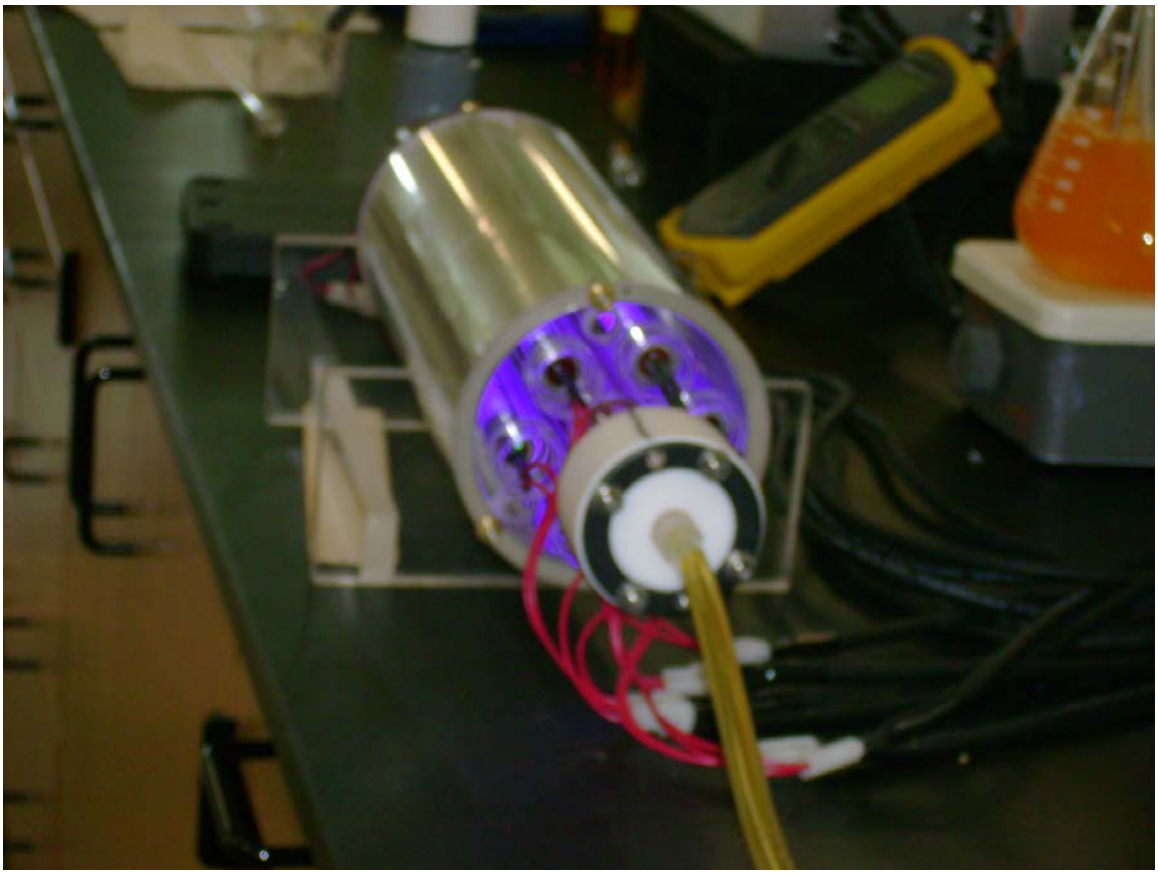

Figure 14 Reactor Casing and UV Light Irradiation

4.7 Experimental Procedures for Photocatalytic Measurements

Photocatalytic experiments were performed using a glass batch reactor system, which was described in detail above. A 20 ppm methyl orange solution using de-ionized water was prepared using (A.C.S. Reagent) MO from Sigma-Aldrich. Methyl orange was dissolved into the solution using a magnetic stirrer for 15 minutes. Samples were drawn and the initial concentration was measured and calculated in accordance with Beers Law using an Ocean Optics USB2000 spectrometer.

Once the 20 ppm solution was prepared, 100 milliliters of the MO solution was reserved in a beaker. The prepared catalyst was ground in a crucible with 2 milliliters of MO solution to de-agglomerate the material. Portions of the reserved MO solutions were added to dilute the catalyst paste that was then poured back into the beaker. This process was repeated with the remaining MO solution until the maximum amount of the catalyst was recovered from the crucible.

To further de-agglomerate the particles and achieve Langmuir equilibrium, the MO-catalyst solution was then sonicated using a Fisher-Scientific Sonic Dismembrator Model 100. Sonication was performed at 5 watts (RMS) for 15 minutes while being magnetically stirred. It is important to note that during this time, adsorption of the pollutant onto the surface of the catalyst also took place altering the initial concentration of the MO solution. The solution was then moved to the experimental area where it again was placed on a magnetic stirrer [6]. Figures 15 shows the experimental set up.

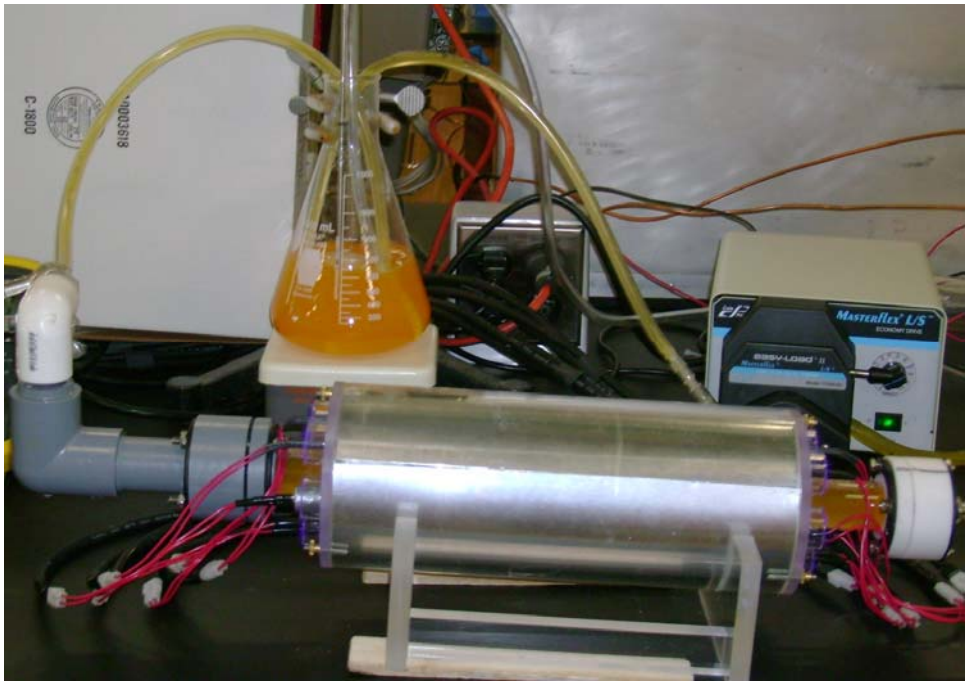

Figure 15 Tubular Reactor Experimental Set Up.

A thermocouple was placed where? to monitor and control the solution temperature. The photocatalytic experiments were conducted in a range from 22°C to 38°C. Breathing Quality Air was used as an oxygen source. The flow rate was controlled by flow meters and bubbled into the solution by aerating stones at a rate of 0.5 liters per minute.

2.0 milliliter samples, representing zero time, were drawn using Micromate 5cc glass syringes and placed into micro-centrifuge tubes. The solution was then irradiated using the light sources detailed above. Spectrum experiments were conducted with duration of three hours. Samples were drawn at 30 minute intervals for the first hour, followed by one hour intervals until the 3 hours were completed.

At the completion of the experiment, the samples collected were centrifuged using an Eppendorf 5414C centrifuge at 8,000 rpm for 10 minutes. The samples were then syringed to new tubes then centrifuged again at 8000 rpm for 10 minutes.

The concentrations of the samples were then calculated by measuring the absorbance of the samples using a spectrometer. The results were compiled and the rate constant for the material was calculated [6].

CHAPTER 5: METHYL ORANGE AS POLLUTANT

Methyl Orange (MO) is a common industrial dye that is categorized as an azo-dye. Azo compounds are synthetic inorganic chemical compounds that account for about 50-70% of the world's production of dyes. In the textile industry, it is estimated that 10–15% of the dye is lost during the dyeing process and released as effluent waste causing contamination [27]. The main problem is that dye wastes can also generate dangerous by-products through oxidation chemical reactions taking place in the wastewater phase or through generation of hazard products in the cleaning process.

The chemical formula and molecular composition for methyl orange is $C_{14}H_{14}N_3SO_3Na$. It is a very stable compound due to the large proportion of aromatics in the dye and the presence of the benzene rings, which keep this pollutant from decomposing easily by chemical or biological methods [6]. In this study, methyl orange was used because of its visible color that allows optical measurements for the evaluation of its degradation. This compound is an acid-base indicator showing orange in basic medium and red in acidic medium.

5.2 TiO_2 Photocatalytic degradation

For the purpose of this thesis, titanium dioxide (TiO_2) was used as a photocatalyst for the detoxification of water containing methyl orange (MO) as a

model compound. The experimental technique for evaluating MO degradation is similar to the experimental technique described by M. Schmidt in his thesis work [6]. The experiments were conducted using de-ionized water as the solvent, to determine the optical absorption spectra of methyl orange. To establish the calibration curves, aqueous solutions of methyl orange were prepared in varying concentrations from 0.3125 ppm to 20 ppm as shown in Figure. 16.

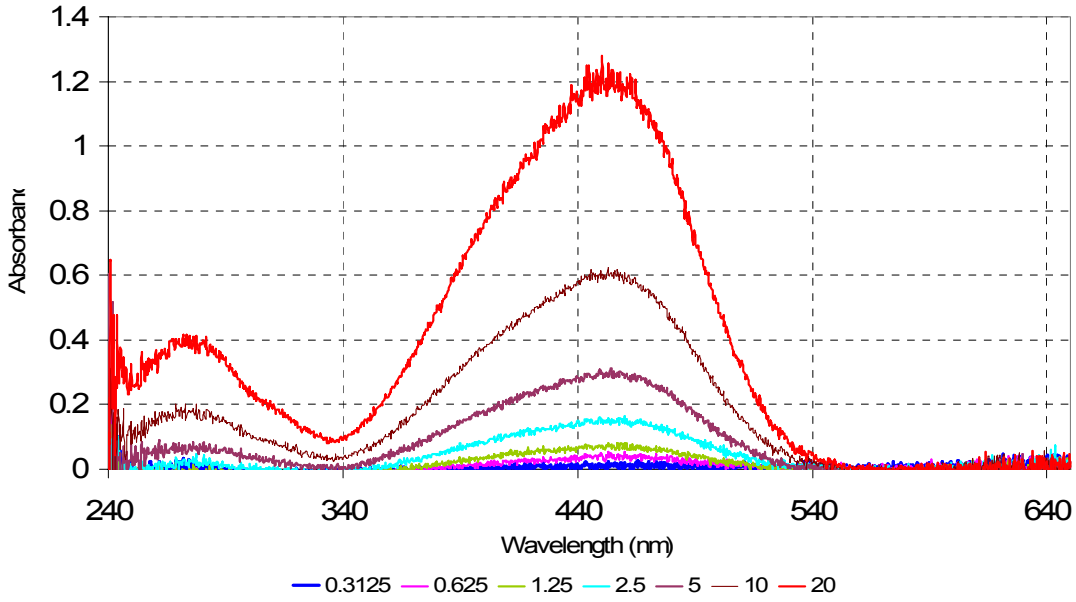

Figure 16. Methyl Orange Optical Absorption Calibration.

For this work the 20 ppm solution was chosen and its spectrum is shown in Figure 17. This chart shows two absorption peak maxima, one at approximately 272 nm and a second with a higher absorption magnitude at 451 nm. Consistent with published work in this area, the second maximum peak at 451 nm was used to calculate the concentration changes as a function of time for

methyl orange [6,15,27]. These peaks and corresponding spectra are in line with published results depicting absorption peaks at 270 nm and 458 nm [20].

UV and fluorescence lights were used as an irradiation source in the experimental set up. An additional test was made to measure the degradation Mo due to TiO_2 without light sources.

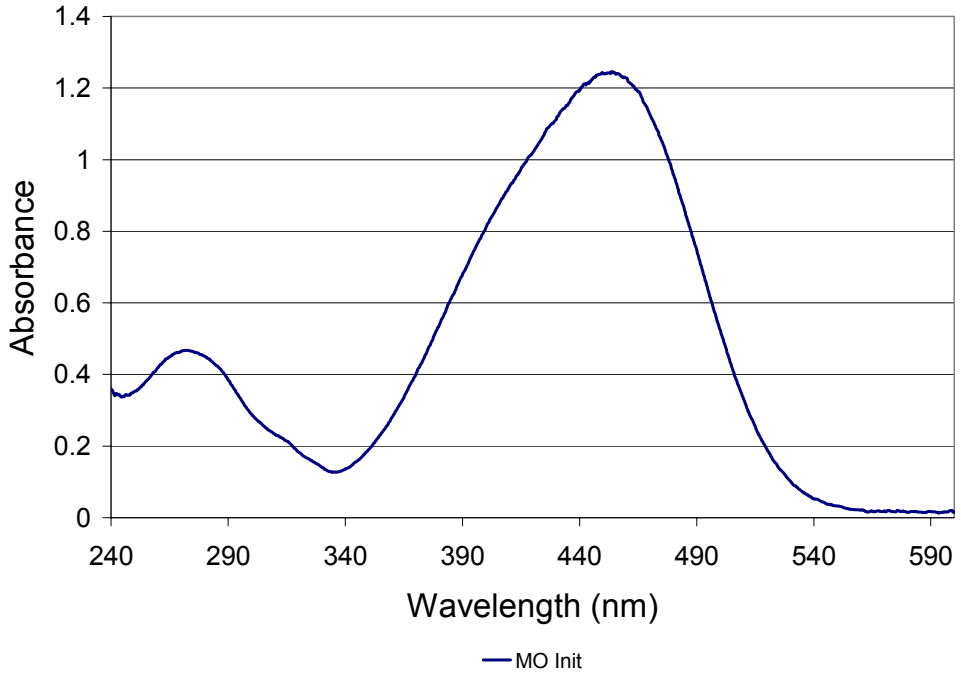

Figure 17. Spectra of 20 ppm Methyl Orange Solution [6]

The test was conducted using a 20 ppm MO solution prepared in a glass beaker loaded with 1 g/L of TiO_2 and stirred in the dark with samples taken after 30 minute intervals. The results are depicted in Fig. 18 and showed that there was no degradation for the MO in the presence of TiO_2.

Consistent with the literature, there was no degradation of the MO in the presence of TiO_2 without UV lights [15, 27] and the complete disappearance of the dye is only observed in the presence of both UV light source (320nm – 400nm) and catalyst (TiO_2). Consistent with Guettai et. al. [27] as well as other published data on the degradation of methyl orange by TiO_2, the peak at 451nm was used as the evaluation point for the absorption measurements of the MO solution.

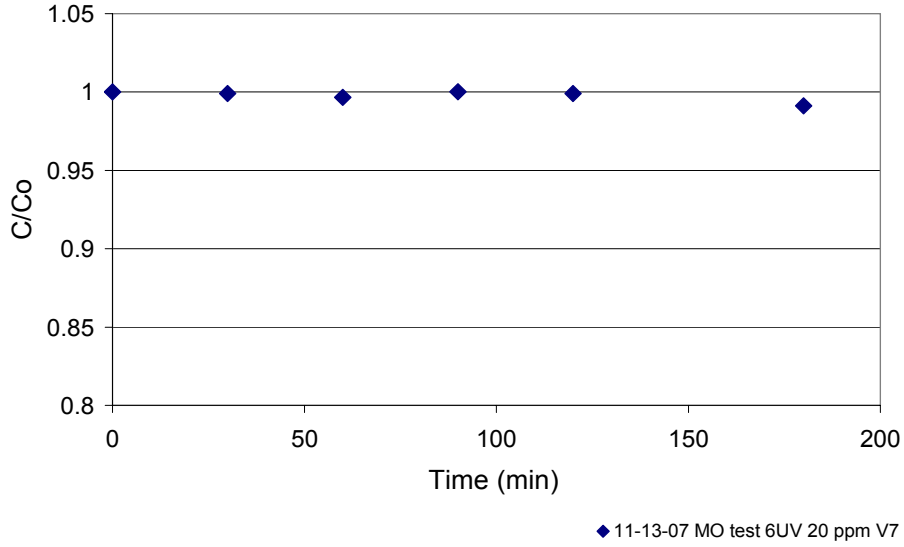

Figure 18. Concentration as a Function of Time for Methyl Orange in the Presence of Degussa P-25 TiO_2 without an Irradiation Source

The value of 451 nm was derived using a box car smoothing method for values between 449-453 nm to account for the fluctuation of data points recorded by the spectrometer at the moment of the measurements. The ratio of the concentration versus initial concentration was then plotted as a function of time.

For the development of the plot of concentration versus initial concentration a rate constant for first order kinetics was calculated. The method used here is similar to the technique employed by both Guettai et al. and Al-Qaradawi et al. for determining rate constants for first order kinetics of the de-colorization of MO [15, 27].

5.3 Catalyst loading

The effect of catalyst loading was tested to determine the optimal loading for both UV light and florescence lights for the tubular reactor designed for this process which will be explained in the following chapters. MO photodegration for different TiO_2 loading was conducted for this study in a natural pH solution. It should also be noted that significant adsorption of the pollutant occurs during the initial 15 minutes of the loading of the MO solution with the catalyst. Therefore, to allow adsorption-desorption equilibration, the solution irradiation by a light source was started with a delay at least 15 minutes in the all experiments described in this work.

5.3.1 UV Light Source

MO photodegradation of TiO_2 was performed using UV lights and a loading in the range of 0.01g/L to 1g/L. The test was conducted using a 20 ppm MO solution prepared in a glass beaker loaded with different amounts of TiO_2 and stirred; samples were taken at 15 minute intervals the first hour and then 30 minutes intervals. The results are depicted in Figure 19.

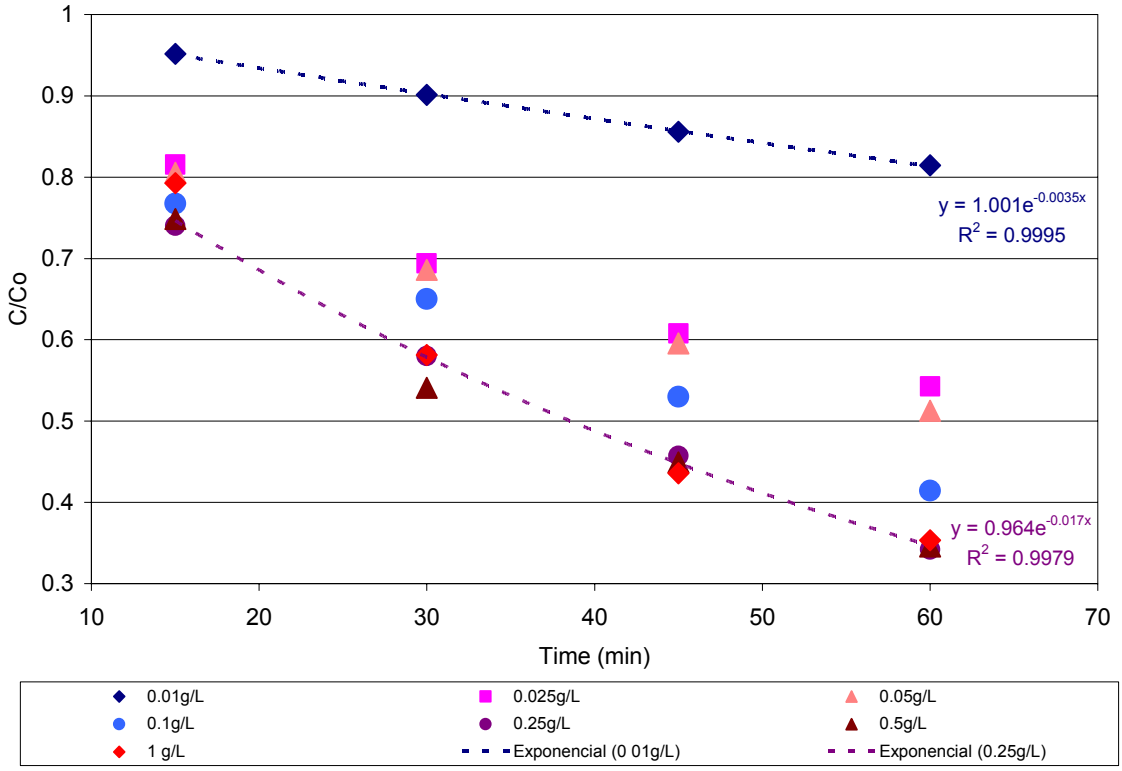

Figure 19. Effects of Catalyst Loading (Grams per Liter) on the Rate of Discoloration for Untreated Degussa P-25 TiO_2 Under UV Irradiation.

The results for the experiments were conducted to find the apparent rate constants for different catalyst loadings for Degussa P-25 TiO_2 under UV irradiation are shown in Figure. 20. From this curve one can see that the degradation rate increases insignificantly as the catalyst loading increases from 0.25 g/L to 1.0 g/L. The optimum catalyst loading found in this study was determined to be 0.25 g/L, with no further increase or decrease in the performance due to increased loading. Choosing an efficient loading is important because an increase in the loading limits the light penetration through the TiO_2 suspension.

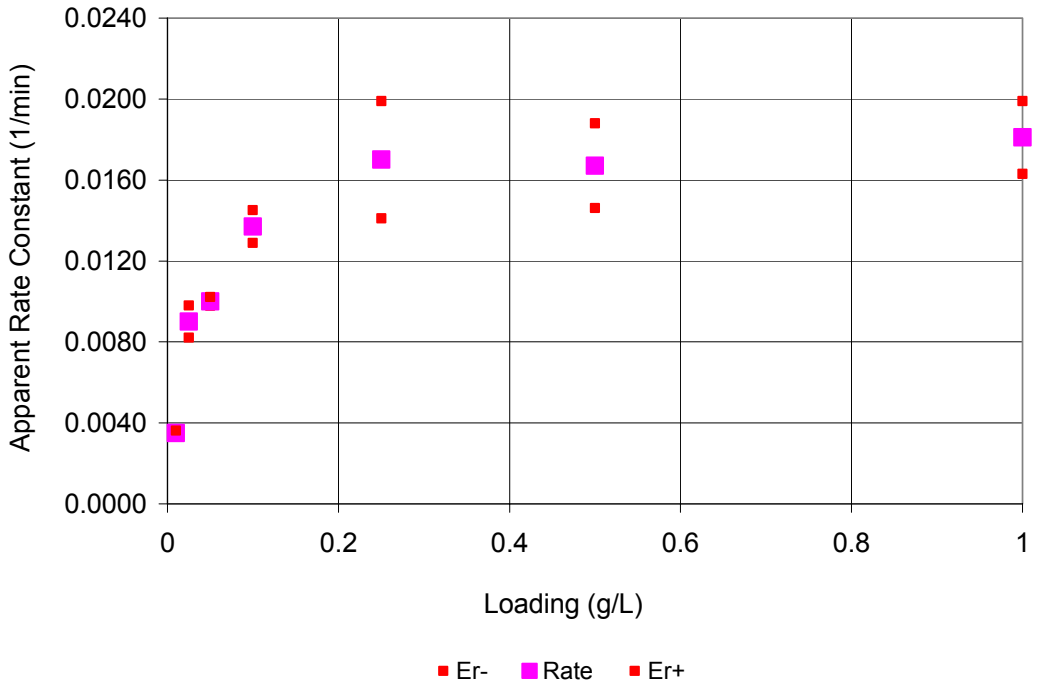

Figure 20. Aparent Rate Constant for Catalyst Loading (Grams per Liter) for Untreated Degussa P-25 TiO_2 Under UV Irradiation

5.3.2 Fluorescence Light Source

MO photodegradation of TiO_2 was also performed using fluorescent light with loading in the range of 0.25 g/L to 4 g/L. The test is similar to the one described in the previous section. A 20 ppm MO solution was prepared in a glass beaker loaded with different amounts of TiO_2 and stirred; samples were taken at 30 minute intervals for the first 2 hours and then at 60 minute intervals. The results are depicted in Figure. 21.

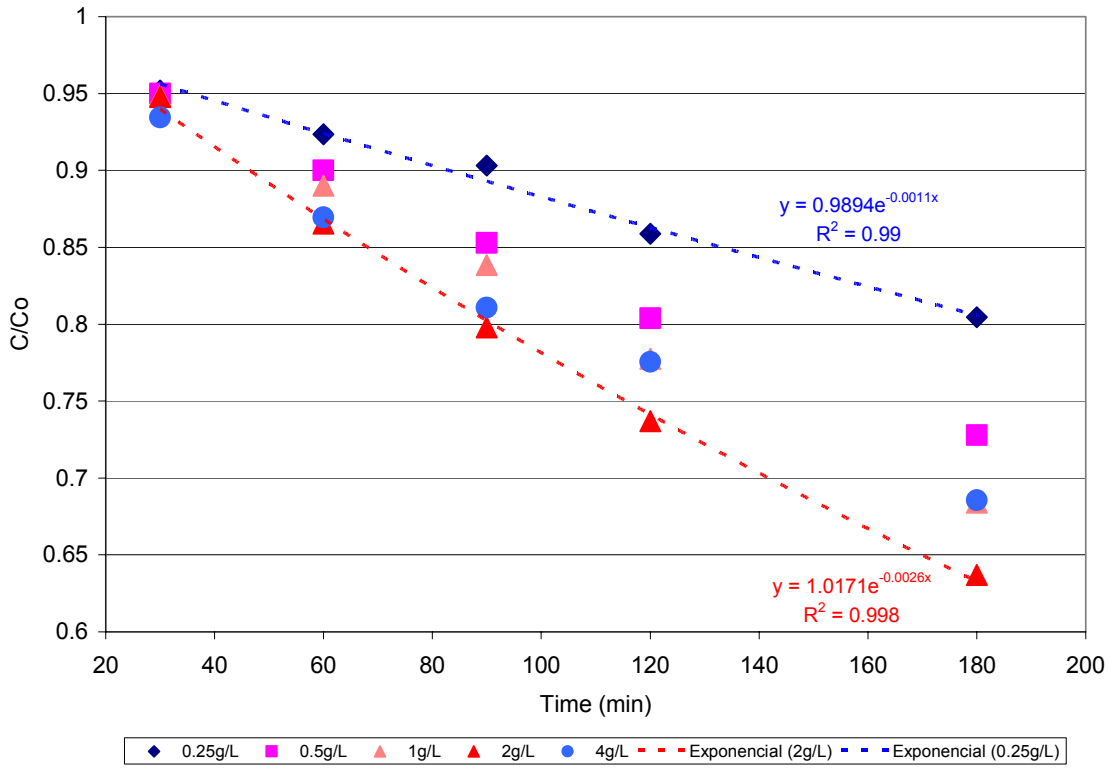

Figure 21. Effects of Catalyst Loading (Grams per Liter) on the Rate of Discoloration for Untreated Degussa P-25 TiO_2 Under Fluorescence Irradiation.

Apparent rate constants for differing catalyst loadings for Degussa P-25 TiO_2 under Fluorescent irradiation are shown in Figure 22. The degradation rate for visible-light increases significantly as the catalyst loading increases from 0.25 g/L to 2 g/L with a further decrease at 4g/L. The results above indicate that the catalyst loading concentration is a function of the type of reactor used, its geometry, type of source and the incident irradiation.

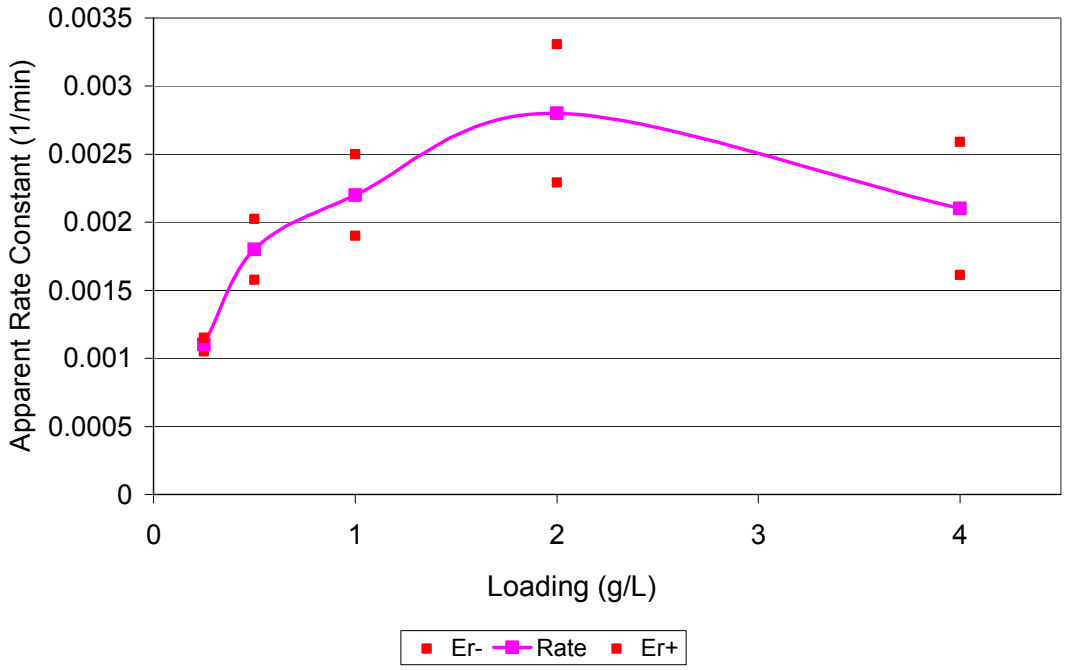

Figure 22 Aparent Rate Constant for Catalyst Loading (Grams per Liter) for Untreated Degussa P-25 TiO_2 Under Fluorescent Irradiation.

Initially, an increase in the concentration of MO increases the probability of a reaction between the pollutant and the oxidizing species. This in turn results in an increase in the discoloration rate. As the concentration of MO increases, the active sites on the catalyst surface are more fully covered reducing the photogeneration of holes or hydroxyl radicals. It has been concluded that the hydroxyl radical is responsible for most heterogeneous photocatalytic oxidations. The hydroxyl radical is formed by the reduction reactions of holes with either water or hydroxide ions [22].

There are many factors that affect the photocatalytic activity of TiO_2. These include the lattice structure and phase of the material, specific surface area, adsorption of the pollutant, electron–hole generation and recombination, carrier lifetime and trapping, solution pH, method of synthesis, catalyst loading, and initial pollutant concentration, among many others. M.Schimdt [6] research showed the profound difference that the design and materials of the reactor itself can have on the photocatalytic effect or rate. The general conclusion is that the optimum catalyst loading is a function of the active surface area and the pollutant concentration, and therefore is not necessarily static [27]. Similarly, Al-Qaradawi et al. also found that an increase in initial catalyst concentration ultimately decreases the overall degradation efficiency [15].

CHAPTER 6: STUDY OF Zn DOPED TiO_2 NANOPOWDERS

The first part of this thesis work explores the effects of Zn doped TiO_2 by the sol-gel method on the photocatalytic activity and the characterization of the doped samples. Since this study is part of a collaborative initiative, the samples have been synthesized and are provided by Dr. A. R. Phani from the Department of Physics, University of L'Aquila. The characterization of the doped and mechano-chemically treated materials will be analyzed by optical diffuse reflectance measurements and optical absorption calculations using the Kubelka-Munk approach. The photocatalytic properties will be studied by the analysis of decomposition of Methyl Orange in an aqueous solution. An aqueous photocatalytic tubular reactor with capability of operation under UV and/or fluorescent light was designed, UV light was used for the Photocatalytic portion of this study.

6.1 Sol gel process on Zn doped TiO_2

Untreated TiO_2 can utilize less than 4% of the available solar energy for photocatalysis. Given the exceptional photocatalytic properties of TiO_2, a great deal of study has gone into decreasing the band gap to allow visible-light activated photocatalysis. Doping TiO_2 by metals or transition metals and anion doping have dominated this area of research. One of the primary goals of this

research was to investigate the characteristics of treated TiO_2 with zinc. If successful it would account for a relatively inexpensive way to lower the band gap of Degussa P-25 TiO_2 and improving its photocatalytic efficiency. Doping TiO_2 can alter the conductivity and optical properties by creating new surface states that are believed to lie near the conduction band or valence band of TiO_2 [5]. Also, doping of TiO_2 with transitional ions offers a way to trap charge carriers and extend the lifetime of both charge carriers. Consequently, dopants enhance the photocatalytic activity [30]

In the present investigation Zn doped TiO_2 nanopowders supplied by Dr. A.R. Phani, have been prepared by simple and cost effective sol-gel process. The sol-gel process has been used to obtain particles with higher purity and homogeneity at lower processing temperatures. Recently, the sol–gel process has become a novel technique for the preparation of nanocrystalline TiO_2. It has been demonstrated that through the sol–gel process, the physico-chemical and electrochemical properties of TiO_2 can be modified to improve its efficiency. It provides a simple and easy means of synthesizing nanoparticles at ambient temperature under atmospheric pressure and this technique does not require a complicated set-up. Since this method is a solution process, it has all the advantages over other preparation techniques in terms of purity, homogeneity and flexibility in introducing dopants in large concentrations, stoichiometry control, ease of processing and composition control [39].

Phani et. al. prepared the samples used for this study using a calculated quantity of titanium dissolved in ethanol (99.98%) solvent along with acetyl-acetone as a chelating agent and cetyltrimethyl ammonium bromide (as surfactant to control the growth of TiO_2 crystallites). This had been dissolved in ethanol solvent in a beaker and the contents were added drop-wise to the titanium butoxide sol under vigorous stirring for 6 hours at room temperature. Calculated quantities of HCl and deionized water were added to increase the rate of reaction [40].

In addition, the contents were refluxed at 60 °C for 4 h to complete the reaction and cooled down to room temperature. The contents were filtered using Whatman filter paper in order to remove any particulates formed during the reaction and then dried at 100 °C for 1h. At the end, the powders were calcined at different temperatures ranging from 500°C to 800°C for 3 h in air in order to enhance the photocatalytic activity. Zn was used to dope (Zn acetate as a source) the TiO_2 base material. Figure 23 shows the flow-chart of the sol gel process [40, 41].

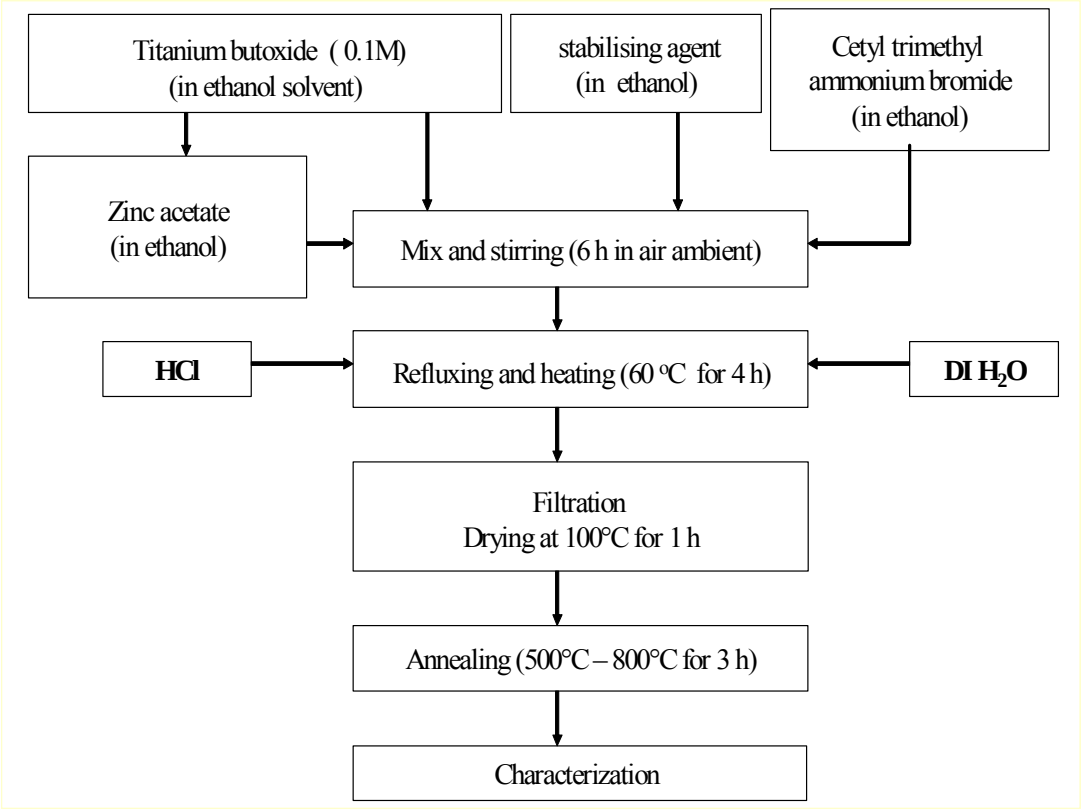

Figure 23 Preparation of Zn Doped TiO_2 Nanopowders by Sol Gel Process [40]

Doping of TiO_2 with transitional ions offers a way to trap charge carriers and extend the lifetime of both charge carriers. Consequently, dopants enhance the photocatalytic activity. Zn doped TiO_2 was prepared with different concentrations of Zn. Table 1 shows the list of the nanopowders received.

6.2 Characterization of TiO_2-Xwt.% Zn Nanopowders

The as-prepared and annealed nanopowders from the process explained above have been examined for their phase identification and surface morphology by employing the X-ray diffraction and scanning electron microscopy (SEM) techniques. Photocatalytic activity studies have been conducted in collaboration

with the information of the samples already sent. The samples received are: TiO_2 nanopowders (sol-gel method) annealed at 500 °C and 600 °C for 3h with a Zn concentration of 1.3 wt%, 2.2 wt%, 3.1 wt%, 4.0 wt%, 4.9 wt%.

6.2.1 X-ray Diffraction Characterization and SEM Measurements

XRD and SEM measurements of the samples were carried out in Italy by Dr. A.R. Phani and are reproduced in Figures 24, 25 and 26.

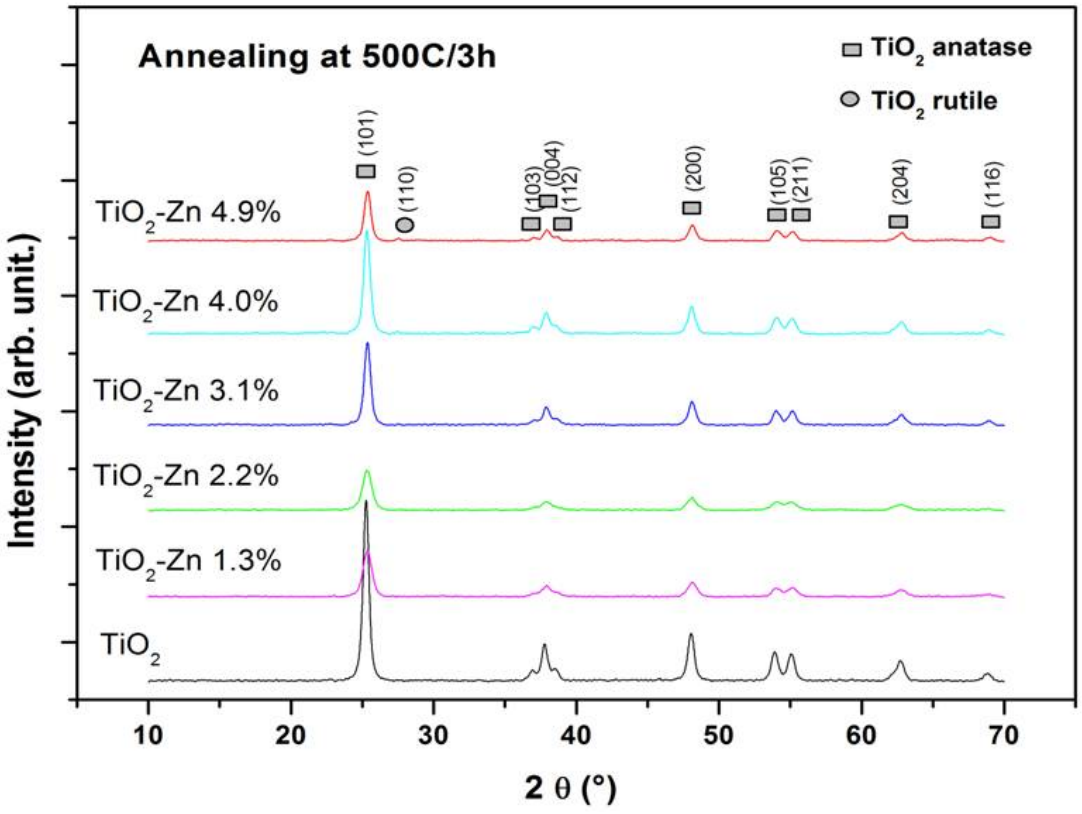

Figure 24. XRD Spectra of TiO2 Zn Annealing at 500°C at 3h [30]

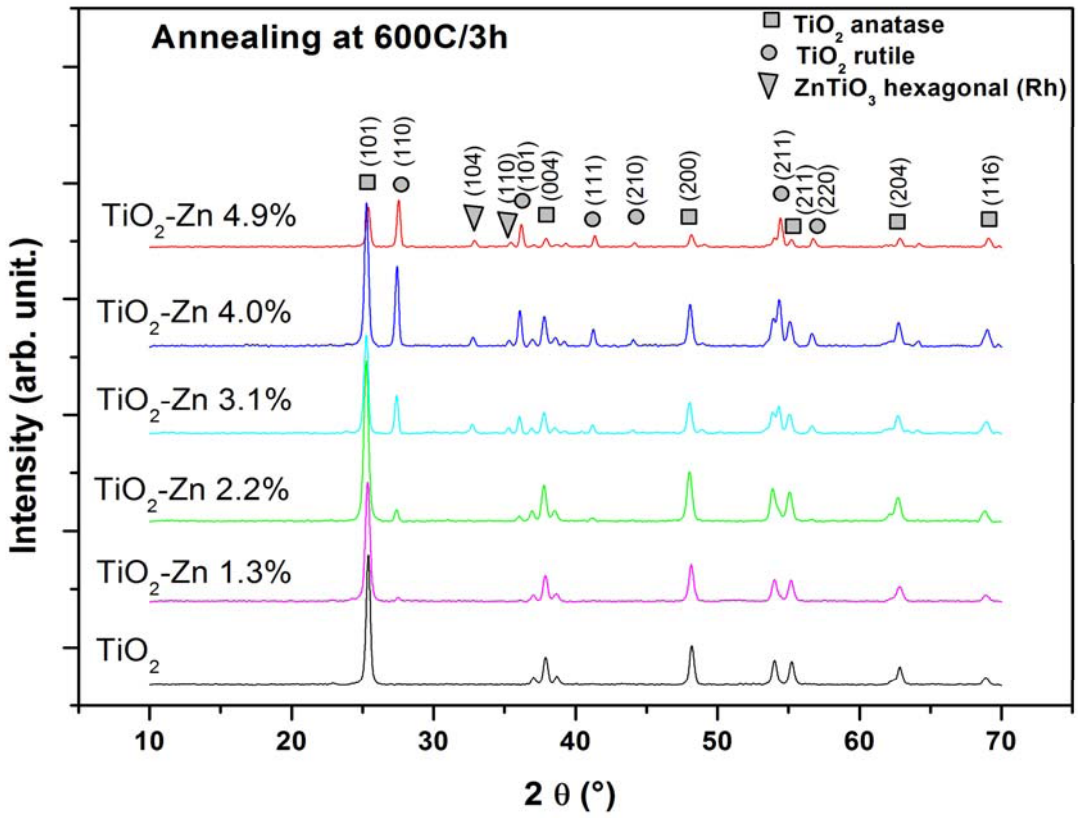

Figure 25. XRD Spectra of TiO2 Zn Annealing at 600°C at 3h [30]

The study of XRD and SEM results by Phani et. al. [30] concluded that pure TiO_2 and Zn doped TiO_2 powders annealed at 500 °C for 3 hours have shown the formation of crystalline phase of anatase TiO_2, independent of Zn concentration. In addition, the variation in the peaks intensity indicates a variation in the anatase phase proportion. The XRD of the nanopowders annealed at 600°C for 3 hours also showed the formation of crystalline phase of anatase TiO_2 accompanied with the formation of rutile phase, the content of which is increased with increasing Zn concentration. In addition, at 3.1wt% and higher,,there exists the formation of $ZnTiO_3$. Phani et. al. [30] concluded that by increasing the Zn concentration (1.3 wt% to 4.9 wt%) the crystallite size of TiO_2 was drastically

reduced from 40 nm to 25 nm and had an effect on the formation of pores with diameter dimensions of 100 -120 nm for the 500°C annealed samples. For the 600 ^{o}C annealed samples the crystallite size of TiO_2 was drastically reduced from 55 nm to 30 nm and was accompanied with the formation of pores with diameter dimensions of 80 -100 nm.

Figure 26 represents the SEM microstructures of TiO_2 doped with different concentrations of Zn. It is clearly seen from these microstructures that particle fragmentation, homogenization and agglomeration effects, at different loading concentrations of Zn, the TiO_2 matrix nanopowder.

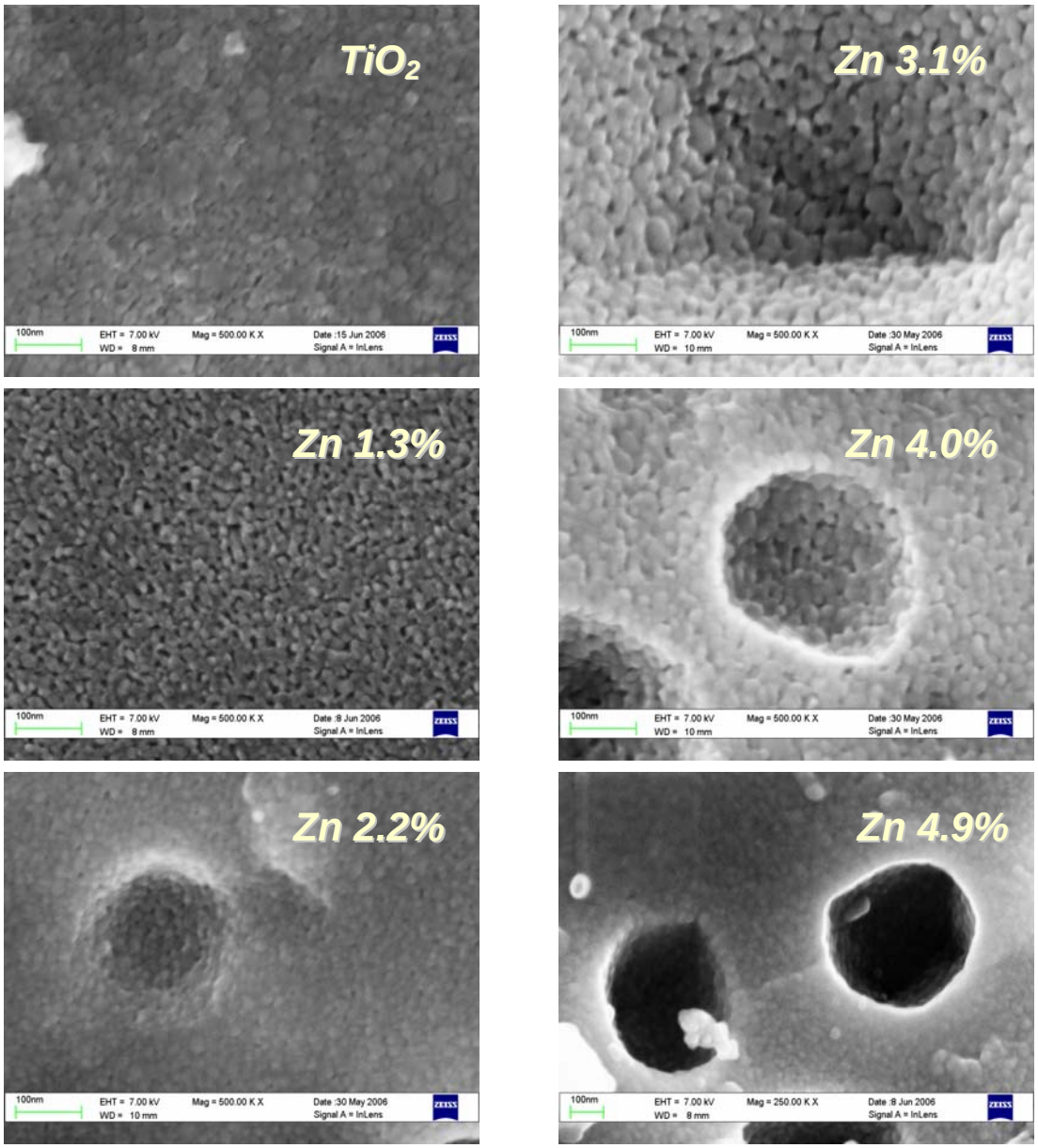

Figure 26. SEM Images of Different Concentrations of Zn Doping of TiO_2 [30]

6.2.2 BET Surface Area Measurements

Autosorb-1C from Quantachrome Instruments has been employed to determine the surface area and pore size distribution of the Zn doped samples. Each of these samples was placed in a glass tube and was out gassed at 300 °C for 3 hours. The external bath for the sample was liquid nitrogen (77 K) and a multi point BET method using nitrogen as the adsorbate gas were used to analyze these samples [36].

Autosorb-1C uses the Brunauer-Emmet-Teller (BET) method for the determination of the surface area of solid materials using the BET equation:

$$\frac{1}{W\left(\left(\frac{Po}{P}\right)-1\right)} = \frac{1}{W_m C} + \frac{C-1}{W_m C}\left(\frac{P}{Po}\right) \quad , \qquad (7)$$

where W is he weight of gas adsorbed at a relative pressure, P/P_o, and W_m is the weight of the adsorbate constituting a monolayer of surface coverage. The term C is a constant related to the energy of absorption in the first adsorbed layer and its value is an indication of the magnitude of the adsorbent/adsorbate interactions [42]. Table 1, shows the surface area of the data collected for the Zn doped samples.

The total pore volume is derived from the amount of vapor adsorbed at a relative pressure close to unity, by assuming that pores are then filled using liquid adsorbate. Figure 27 and Figure 28 show the relationship between pore diameter and total pore volume of the samples. The pore volume of TiO_2-Xwt.% Zn varies

with the value of X. For X=1.3 wt.% (lower doping level of Zn), the pore volume increases two times when compared to pure TiO_2, however, it decreases with an increase in concentration of Zn. The pore diameter of around 18-20 Å was uniformly obtained irrespective of the Zn concentration in the sample.

Table 1 BET Surface Area Results

Sample #	Description	Surface Area (m^2/g)
8	Nanopowders (sol-gel) 500C 3h	33.27
9	Nanopowders (sol-gel) 1.3% 500C 3h	73.14
10	Nanopowders (sol-gel) 2.2% 500C 3h	40.80
11	Nanopowders (sol-gel) 3.1% 500C 3h	37
12	Nanopowders (sol-gel) 4.0% 500C 3h	53.98
13	Nanopowders (sol-gel) 4.9% 500C 3h	35.18
14	Nanopowders (sol-gel) 600C 3h	12.48
15	Nanopowders (sol-gel) 1.3% 600C 3h	26.41
16	Nanopowders (sol-gel) 2.2% 600C 3h	15.81
17	Nanopowders (sol-gel) 3.1% 600C 3h	13.68
18	Nanopowders (sol-gel) 4.0% 600C 3h	17.80
19	Nanopowders (sol-gel) 4.9% 600C 3h	13.14

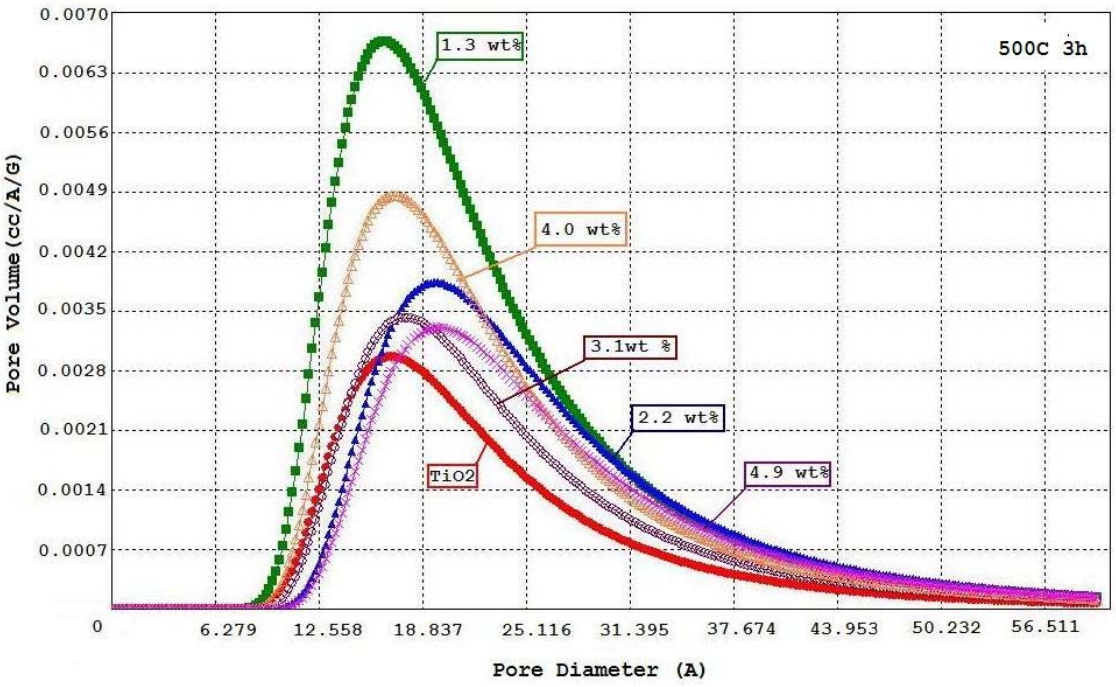

Figure 27. Pore Volume vs Pore Diameter of Zn Doped TiO_2 Annealed at 500°C 3h

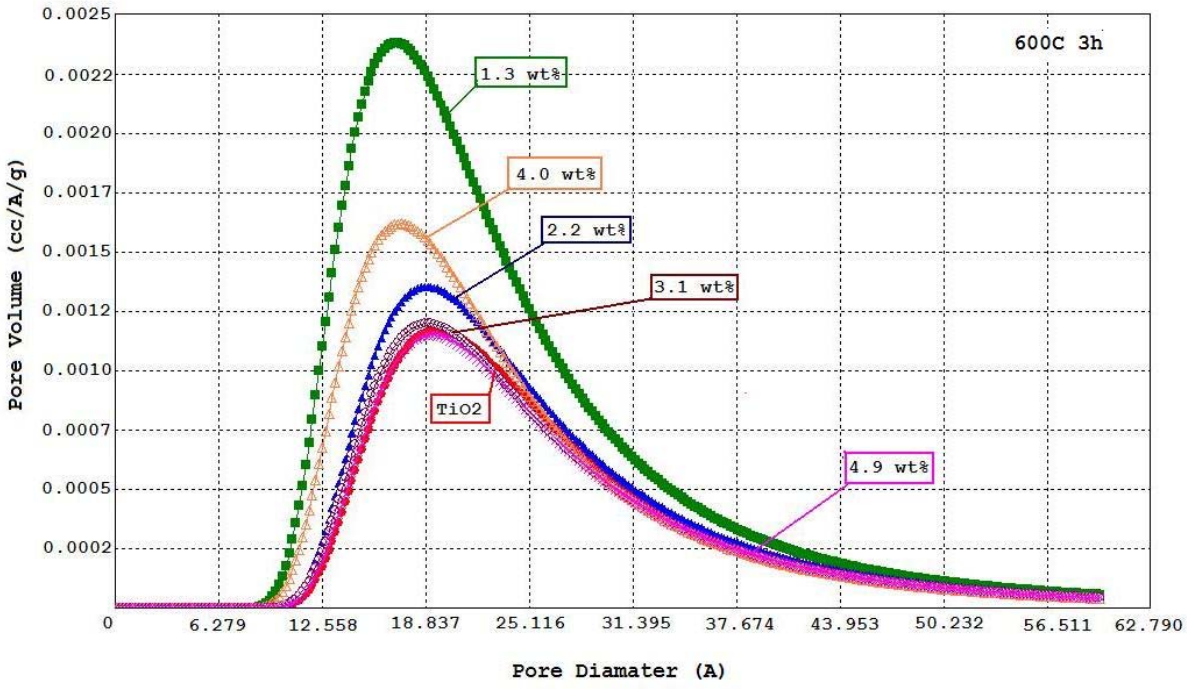

Figure 28. Pore Volume vs Pore Diameter of Zn Doped TiO_2 Annealed at 500°C 3h

6.3 Photocatalytic Activity of TiO_2 Nanopowders

Photocatalytic activity for this study was performed using a Tubular Reactor and 6 UV lights, the experimental set up will be explained in the following chapters. Methyl Orange is the pollutant of choice; its degradation in the suspension with the photocatalyst is shown in the initial stages of the reaction (during the first two hours). Figures 29 to 31 show the plots for photocatalytic degradation of methyl orange using TiO_2 with different Zn doping concentration. Both 500°C and 600°C annealed photocatalysts revealed relatively low photocatalytic efficiency as compared to the industrial TiO_2 P-25 Degussa catalyst (see Figures. 30 and 32). This may be due to the different preparation conditions and the obtained phase proportion of anatase TiO_2 structure.

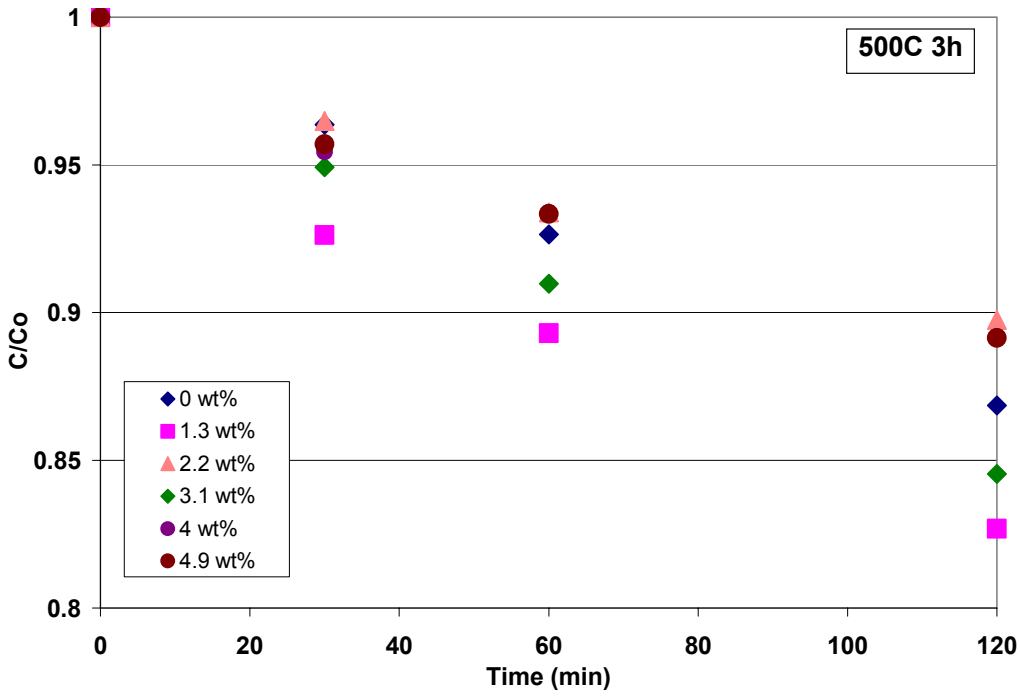

Figure 29 MO Photodegradation of TiO_2 Zn 500C 3h

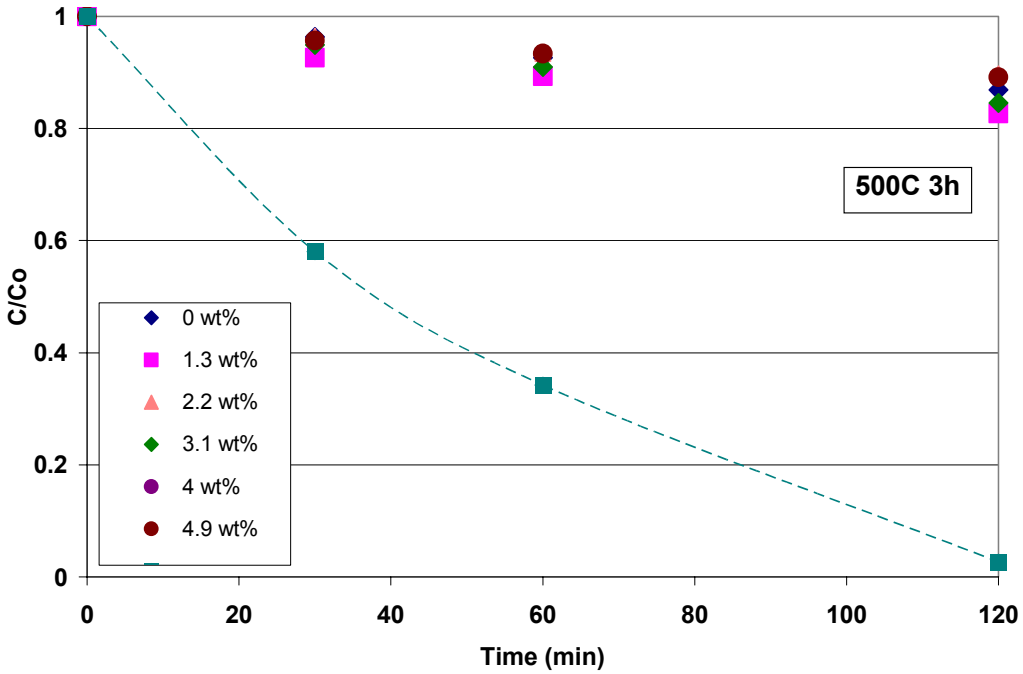

Figure 30. Comparision of Photocatalytic of TiO2 Degussa and TiO2 Zn 500C 3h

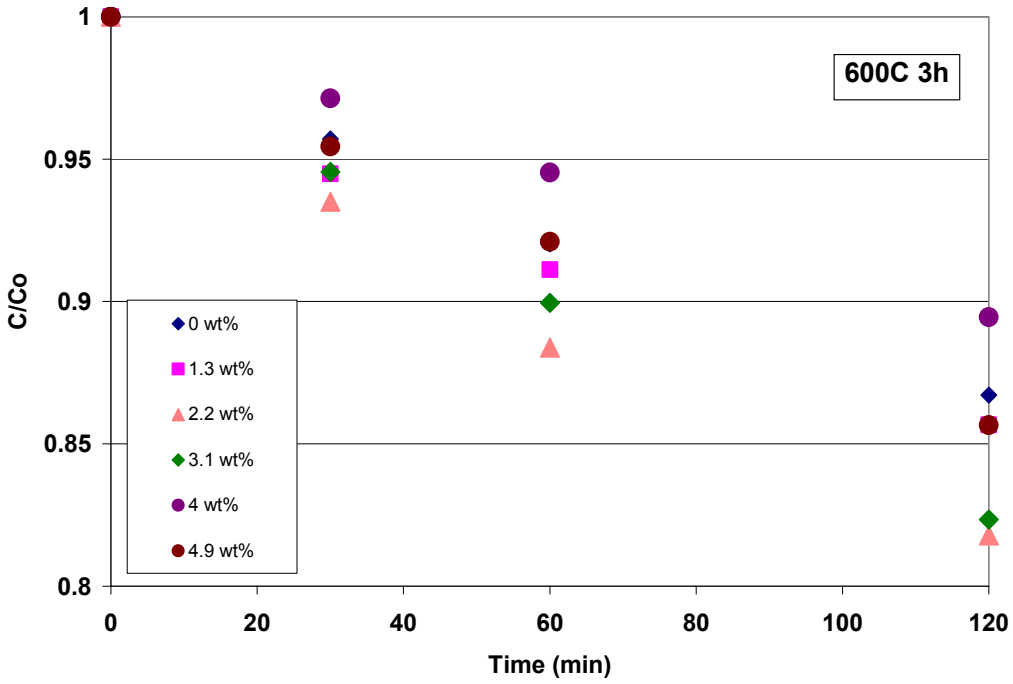

Figure 31 MO Photodegradation of TiO_2 Zn 600C 3h

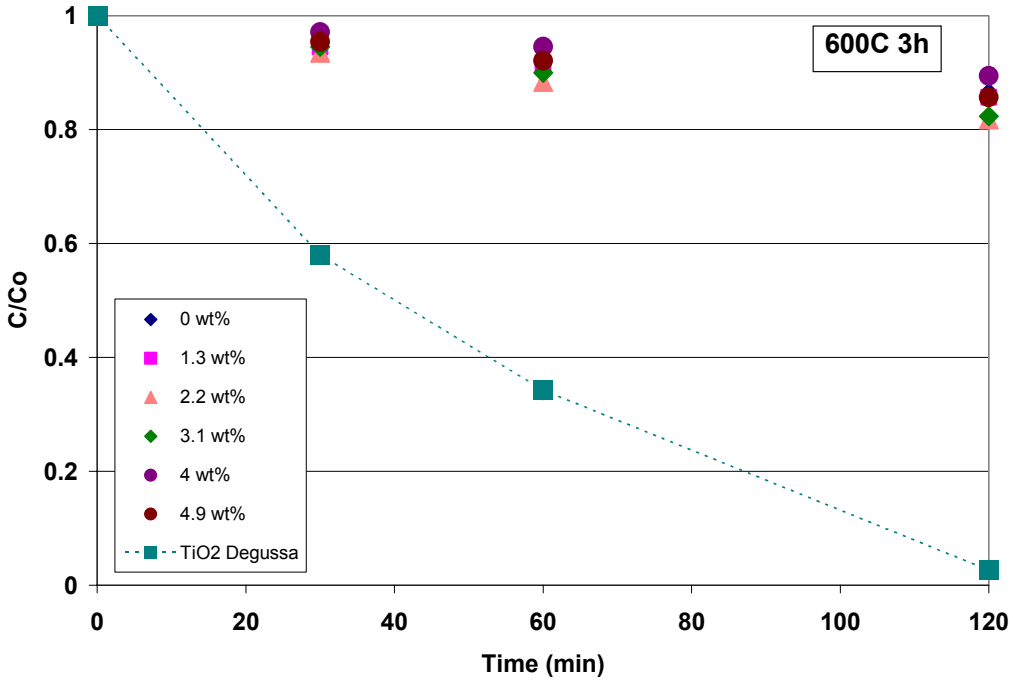

Figure 32. Comparision of Photocatalytic of TiO_2 Degussa and TiO_2 Zn 600C 3h

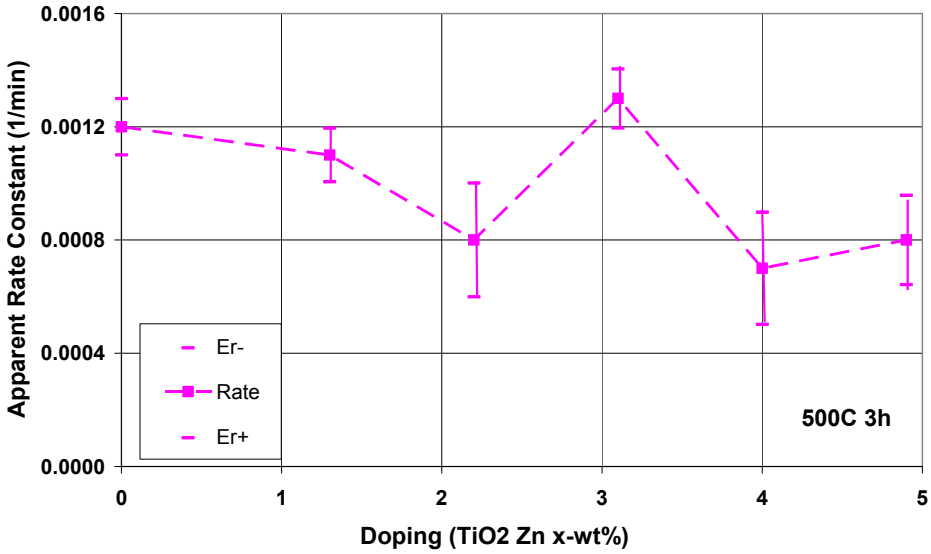

Figure 33. Apparent Rate Constant for Zn Doped TiO_2 500C 3h using a Tubular Reactor and a UV Light Irradiation

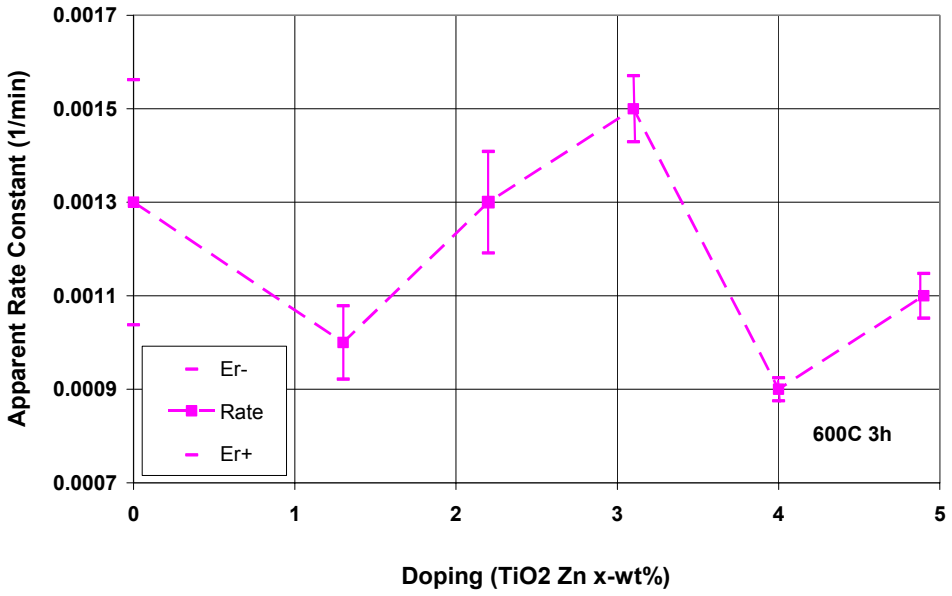

Figure 34 Apparent Rate Constant for Zn Doped TiO_2 600C 3h using a Tubular Reactor and a UV Light Irradiation

The results above (Figures 30 and 32) show that the TiO_2-Zn doped photocatalysts prepared by the sol gel method show lower performance compared to TiO_2 Degussa. There is no significant variation in the photocatalytic materials prepared with the increased Zn correlation. In addition, there is no significant difference in the performance of the photocatalysts prepared by and annealed at 500C and 600C; nevertheless the samples have different phase content (anatase at 500C and anatase+rutile at 600C).

In addition, we can notice that the optical absorption measurements of 3.1 wt.% Zn 500C material do not exhibit any changes in the bandgap as compared to the undoped TiO_2 (Figure 35). However, for 600°C, 3.1 wt% Zn TiO_2, there is a

red shift in the band gap of the doped material, which can be seen in Figure 36. Such a difference in the effect of the annealing temperature can be explained by the presence of the rutile phase in the samples annealed at 600C.

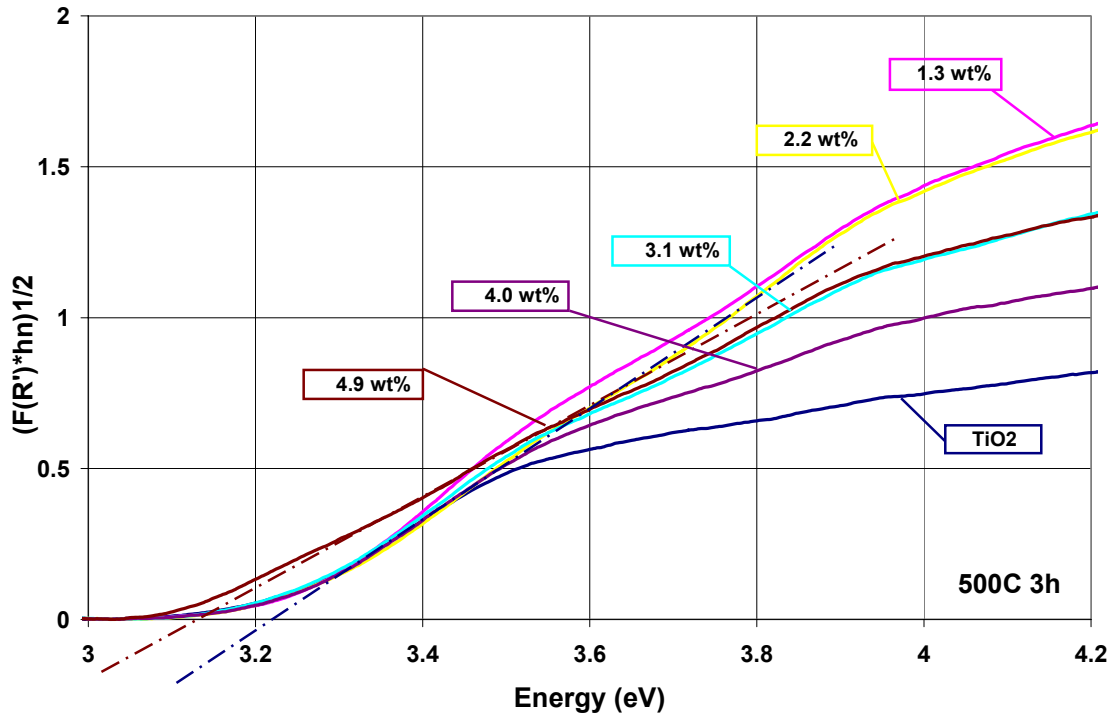

Figure 35. Plot of Optical Absorption (F(R')*hν)1/2 vs. Incident Photon Energy, hν, for the Sol Gel Samples Annealed at 500C.

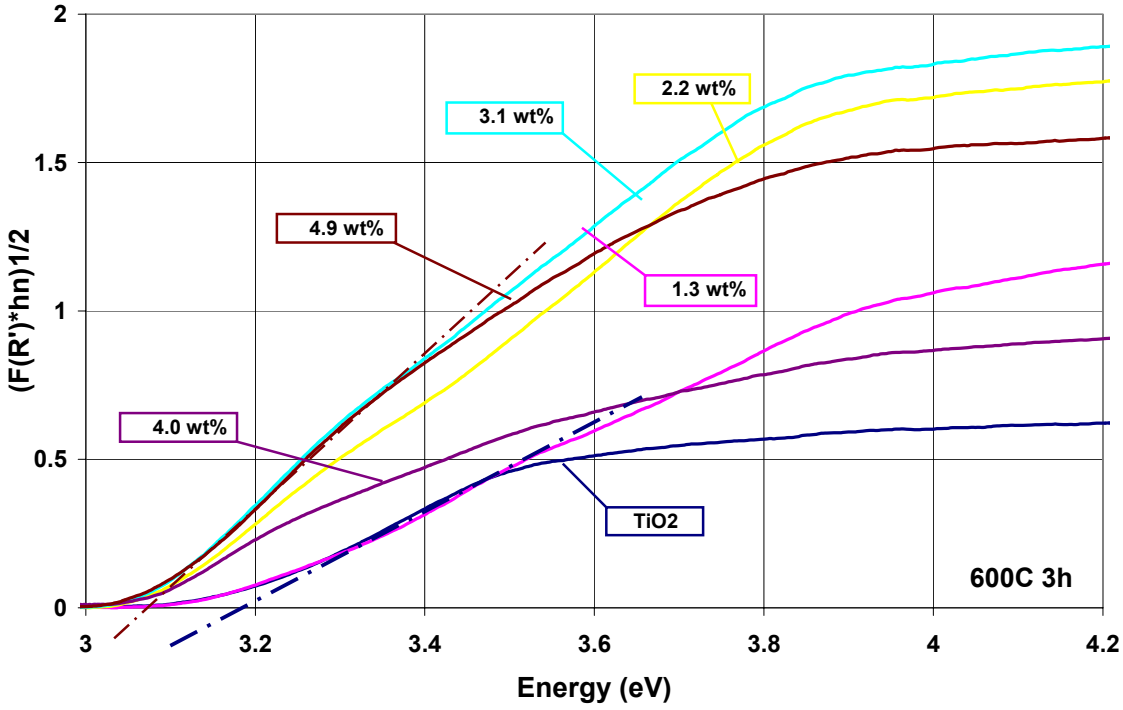

Figure 36. Plot of Optical Absorption (F(R')*hν)1/2 vs. Incident Photon Energy, hν, for the Sol Gel Samples Annealed at 600C.

The results described in this chapter indicate that there is no significant change in the photocatalytic efficiency for TiO_2-X wt.% Zn at two different calcination temperatures (500 and 600 ^oC). The reason for this may be due to the large crystallite sizes and the lower surface area of these initial samples observed from XRD and BET analysis. In the next chapter, we will describe our strategy to improve photocatalytic properties of sol gel Zn doped TiO_2 materials.

CHAPTER 7: BALL MILL INDUCED TRANSFORMATIONS

Researchers are interested in the application of nanomaterials to environmental applications. Nanocrystalline materials exhibit a variety of unique properties, such as high surface area, short interface migration distance and visible light activity that can enhance photocatalytic performance [39]. The sol–gel process is considered to be a novel technique for the preparation of nanocrystalline TiO_2 and it has been demonstrated that by using this technique the physico-chemical and electrochemical properties of TiO_2 can be modified to improve photocatalytic efficiency [39].

In this study, an attempt has been made to enhance the photocatalytic activity of Zn doped TiO_2 by variying the calcination temperature at different concentrations. However, as it was shown in the previous chapter, Zn doping has not demonstrated a significant change in the photocatalytic efficiency of TiO_2-X wt% Zn compared to the regular TiO_2. In this chapter, we discuss a. new strategy for the modification of the catalysts, namely the mechano-chemical milling of TiO_2-X wt% Zn materials in a high energy planetary mill. As it will be seen below, this procedure can optimize the micropore size distribution and increase the surface area of the photocatalytic material.

7.1 High Energy Ball Mill

McCormick et. al. [43], explains that Ball Mill can be defined as a mechano-chemical process (MCP) that uses mechanical energy to activate chemical reactions and structural changes. It has been demonstrated that the activation of chemical reactions by mechanical energy can lead to many interesting applications, like waste processing. High energy ball milling is an alternative technique to obtain nanosized materials through the application of high pressure.

The objectives of the ball milling process include particle size reduction, mixing or blending, and particle shape changes. The most common mill used for these purposes has been a planetary ball mill; a bowl sits on a grinding platform and rotates in a direction opposite to the direction of the base fixture. This action is a lot like the "teacup and saucer" rides commonly found in amusement parks. In planetary action, centrifugal forces alternately add and subtract. The grinding balls roll halfway around the bowls and then are thrown across the bowls, impacting on the opposite walls at high speed. Grinding is further intensified by interaction of the balls and sample. Planetary action gives up to 10g acceleration [34]. The schematic cross-section of the planetary ball mill principle is illustrated in Figure 37,

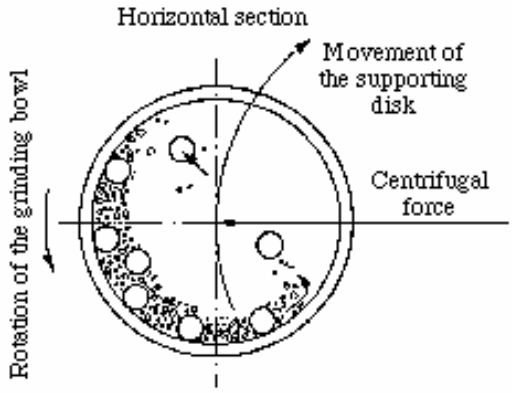

Figure 37. Schematic Cross-section of a Planetary Ball Mill [52]

The mechano-chemical milling of semiconductor oxide materials, particularly TiO_2 and its photocatalytic behavior has been extensively investigated in the past years. Mechanochemical milling is known to generate accumulations of defects, particle size reduction and local temperature increases which contribute to the activation of solid compounds so that they store additional energy which facilitates chemical reactions or transformations [43].

Another important factor in the success of this instrument is its economy; it is an inexpensive and rapid process when compared with other synthesizing methods such as induction melting, quenching, sintering, etc. The present study shows the effect of the ball-mill process on the photocatalytic activity of TiO_2-X wt% Zn samples, which was evaluated by the photocatalytic oxidation of methyl orange as a model organic compound. Pore size, surface area, crystallite size and phase formation are parameters that were studied in this work.

7.2 Ball Milling Transformation of TiO_2-X wt% Zn

Many studies have reported the relation between crystallographic structure and surface properties and the effect of these properties on the catalytic properties of TiO_2 [45–47]. We noticed that Zn doped TiO_2 composite materials prepared by sol-gel method and annealed at 500°C and 600°C were agglomerated in relatively large (crude) dense particles. Therefore, we treated these samples by the ball milling process for 2h. Our preliminary results indicate that wet mechano-chemical synthesis increases the surface area as well as improves the photocatalytic activity of the Zn doped TiO_2 samples, as it is seen from the results below.

Figure 38-41 show plots of photocatalytic degradation of methyl orange using TiO_2 with different Zn doping concentration. Both 500°C and 600°C annealed photocatalysts revealed lower photocatalytic efficiency as compared to the industrial TiO2 P-25 Degussa catalyst (see Fig. 39 and 41).

However, from Figs. 42 and 43, one can see that the rate of degradation of methyl orange in an aqueous solution is more than 2 times higher as compared with the unmodified catalyst. The ball milling process results show a two fold increase in the average improvement of the photocatalytic activity, which can be related to an increase in the surface area and a decrease in the crystal size by the same proportion.

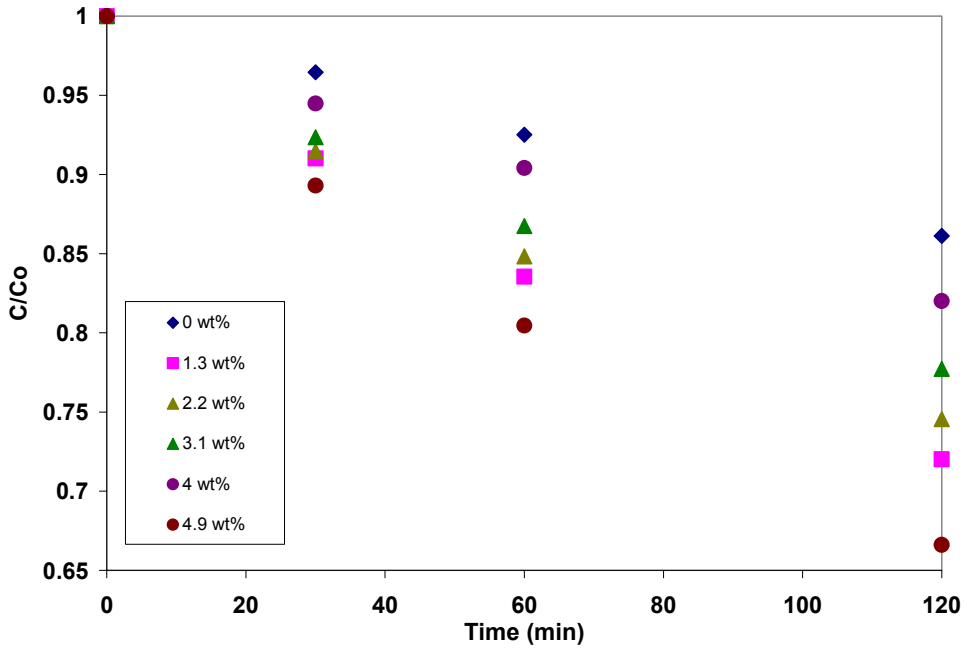

Figure 38. MO Photodegradation of TiO_2 Zn 500C 3h After Ball Milling for 2h.

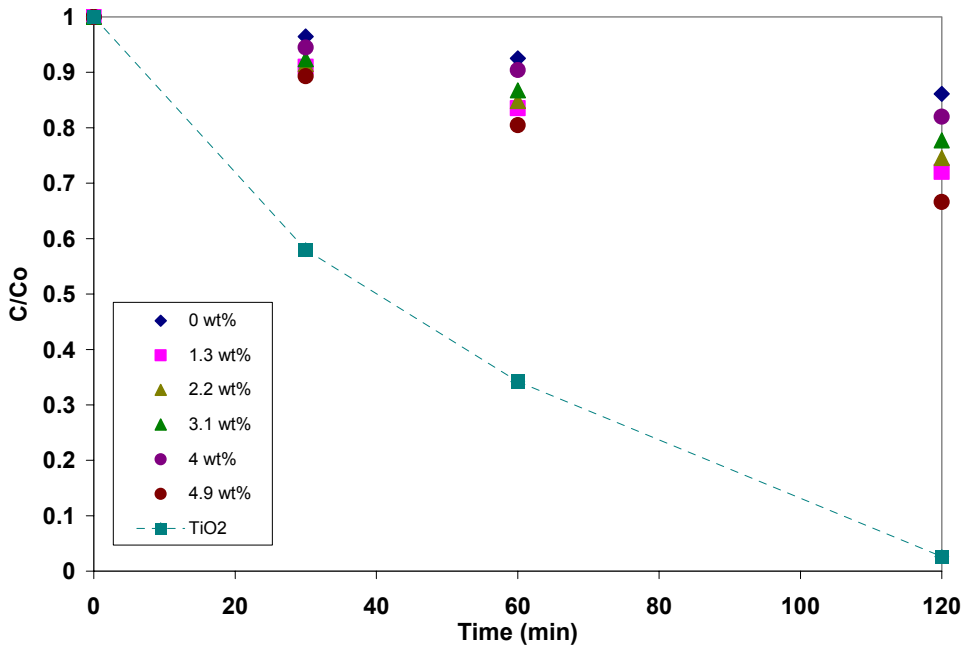

Figure 39 Comparision of Photocatalytic activity of TiO_2 Degussa and TiO_2 Zn 500C 3h After Ball Milling for 2h

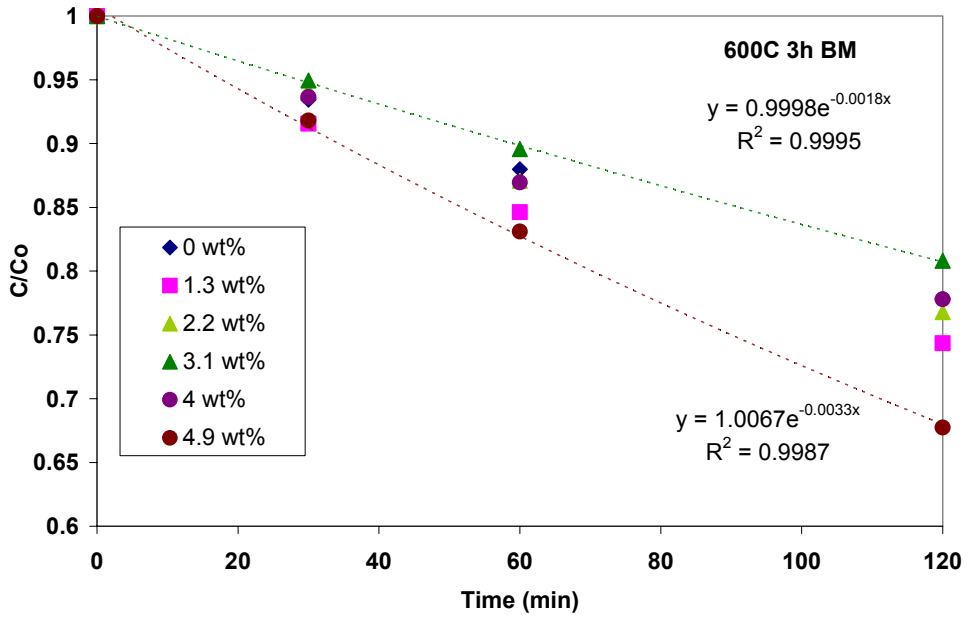

Figure 40. MO Photodegradation of TiO_2 Zn 600C 3h After Ball Milling for 2h.

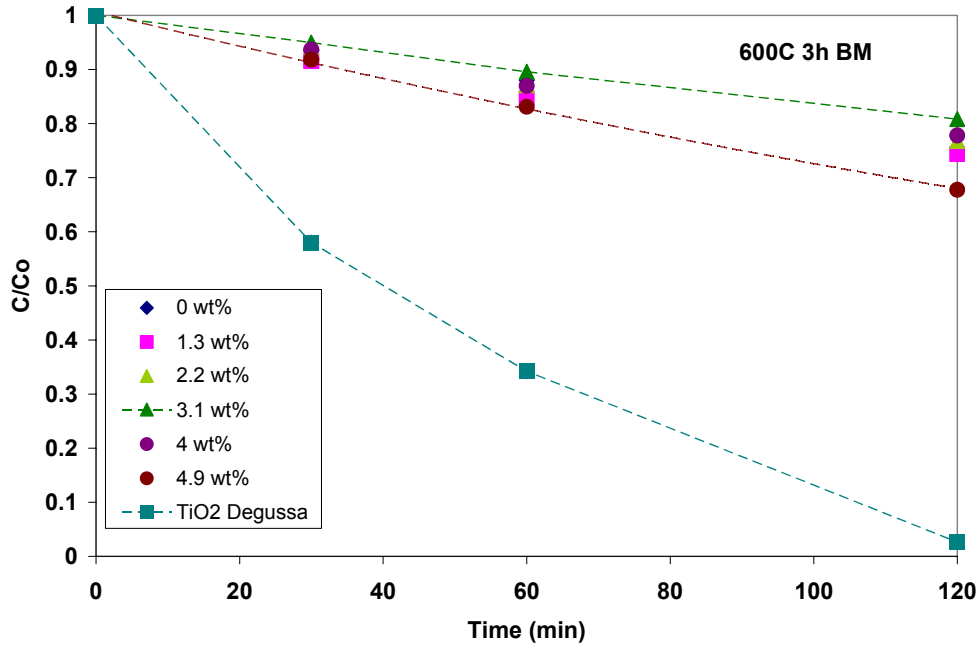

Figure 41. Comparision of Photocatalytic Activity of TiO_2 Degussa and TiO_2 Zn 600C 3h After Ball Milling for 2h

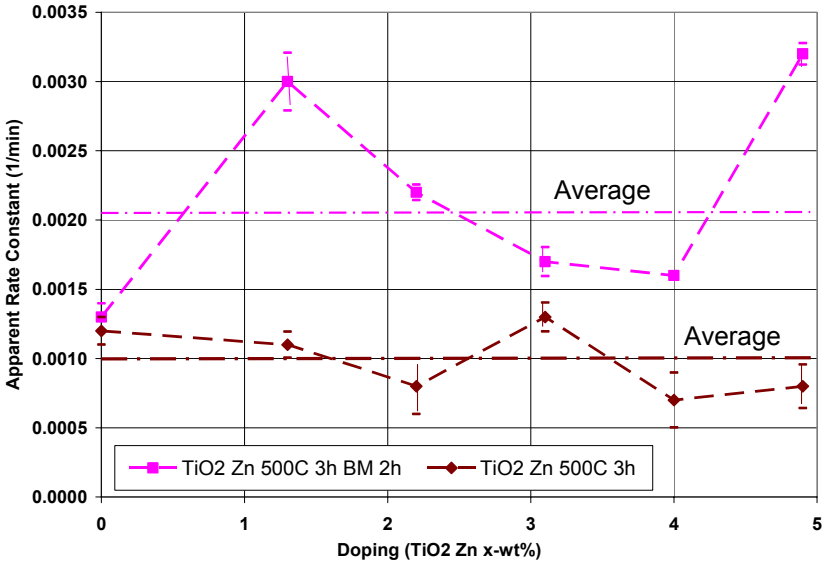

Figure 42. Apparent Rate Constant for Zn doped TiO_2 500C 3h Before and After Ball Milling, using a Tubular Reactor and a UV Light Irradiation.

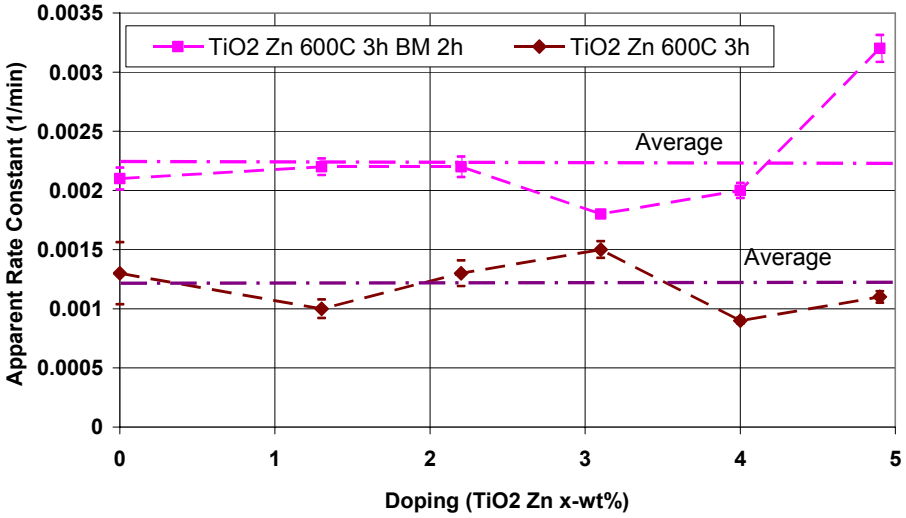

Figure 43 Apparent Rate Constant for Zn doped TiO_2 600C 3h Before and After Ball Milling, using a Tubular Reactor and a UV Light Irradiation.

These results are supported by the decrease of the crystalline particle size obtained by XRD measurements (see Figures. 44-45) that correlate with the apparent rate constants of Figures. 42 and 43. For an increase in surface area there is a decrease of particle size as can be seen in Figure. 46 when compared with Figures. 42 and 43, respectively.

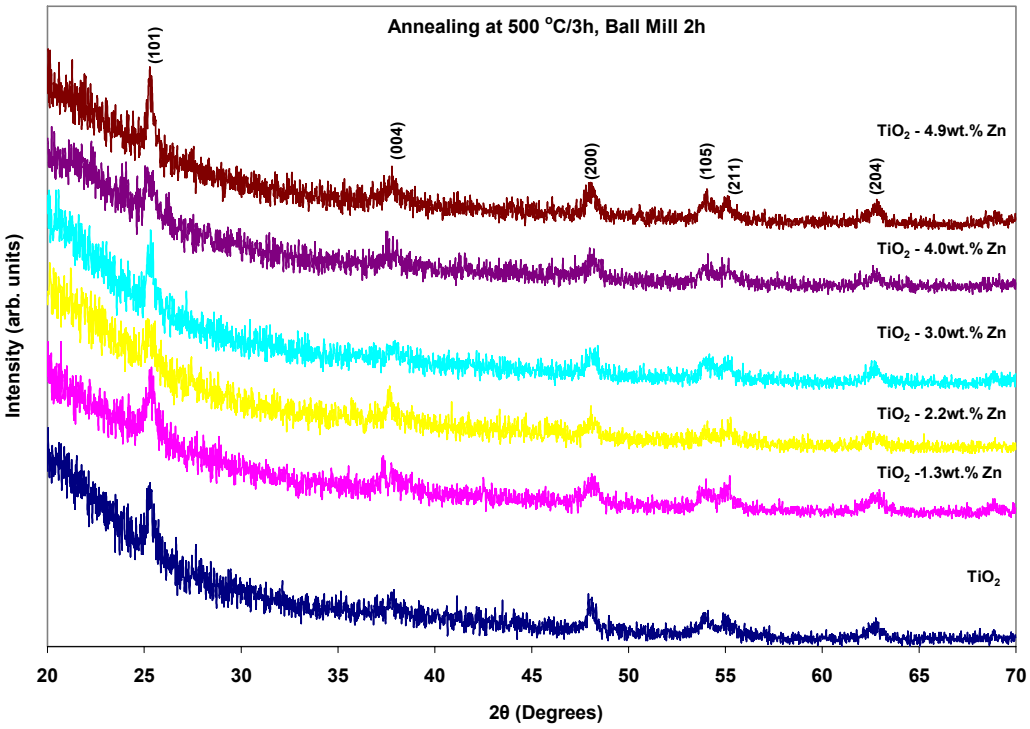

Figure 44. XRD Spectra of TiO2 Zn Annealing at 500°C 3h After Ball Milling

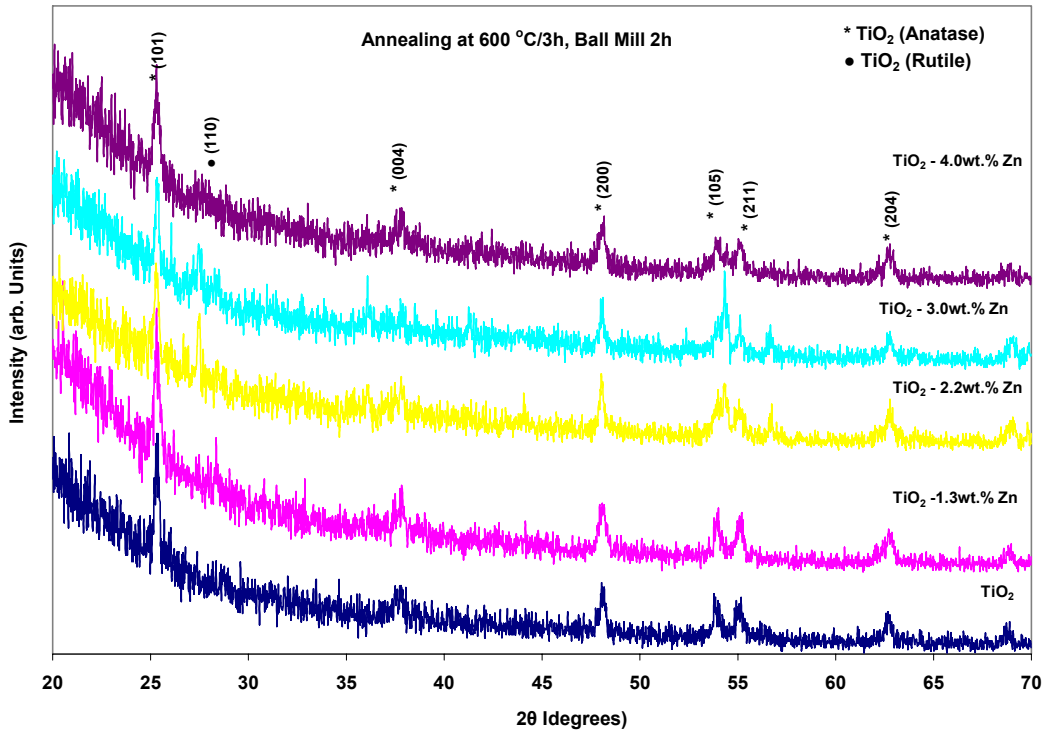

Figure 45. XRD Spectra of TiO_2 Zn Anneling at 600°C 3h After Ball Milling

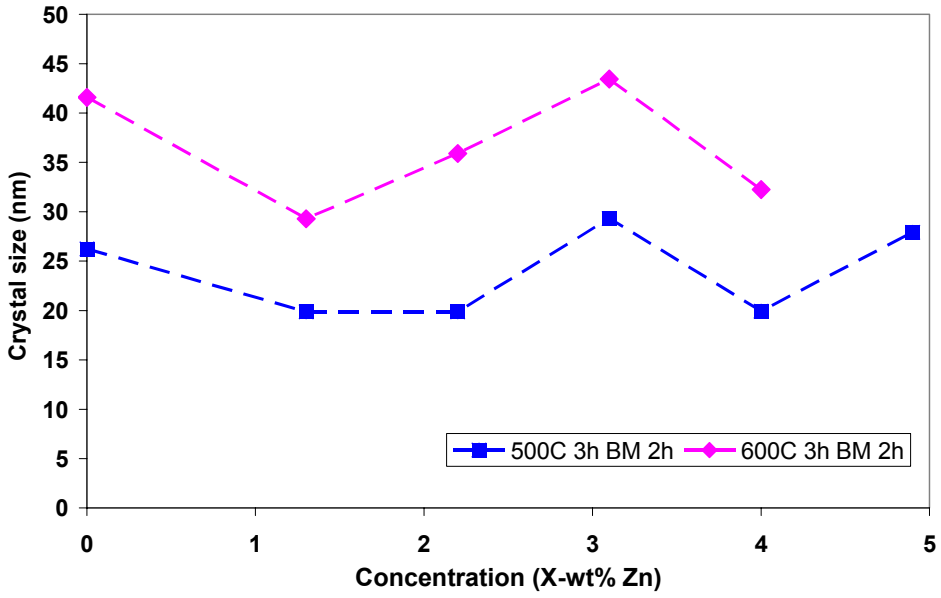

Figure 46 Crystall Size Concentration for 500C and 600C After Ball Milling.

These results seems to be a good agreement between increasing BET surface area and pore size distribution of ball milled samples as shown in Fig. 47-50.

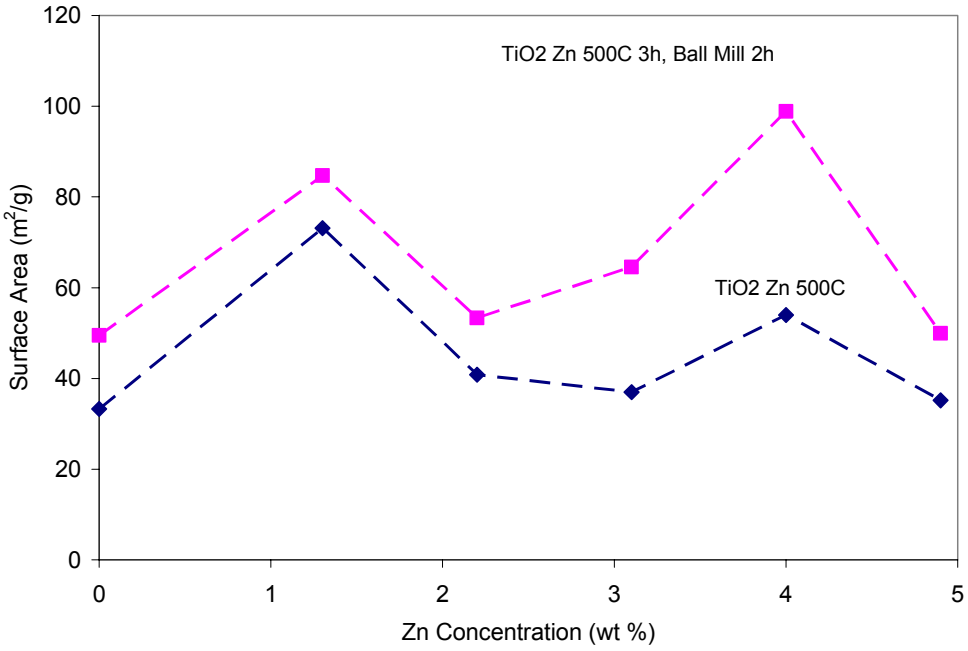

Figure 47. Comparision BET Surface Area Measurement Before and After Ball Milling for 500C 3h

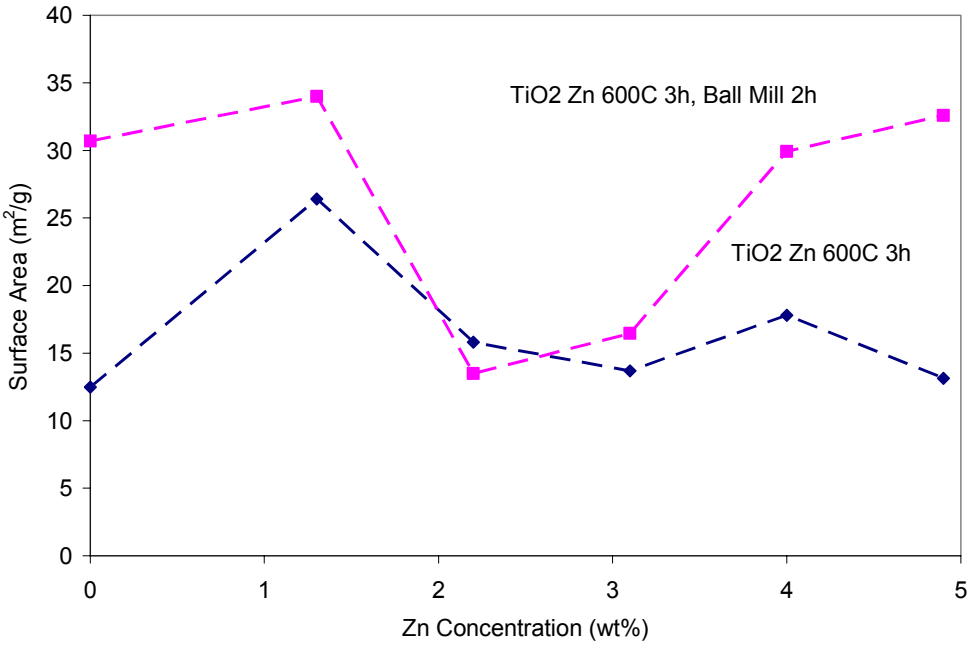

Figure 48. Comparision BET Surface Area Measurement Before and After Ball Milling for 600C 3h

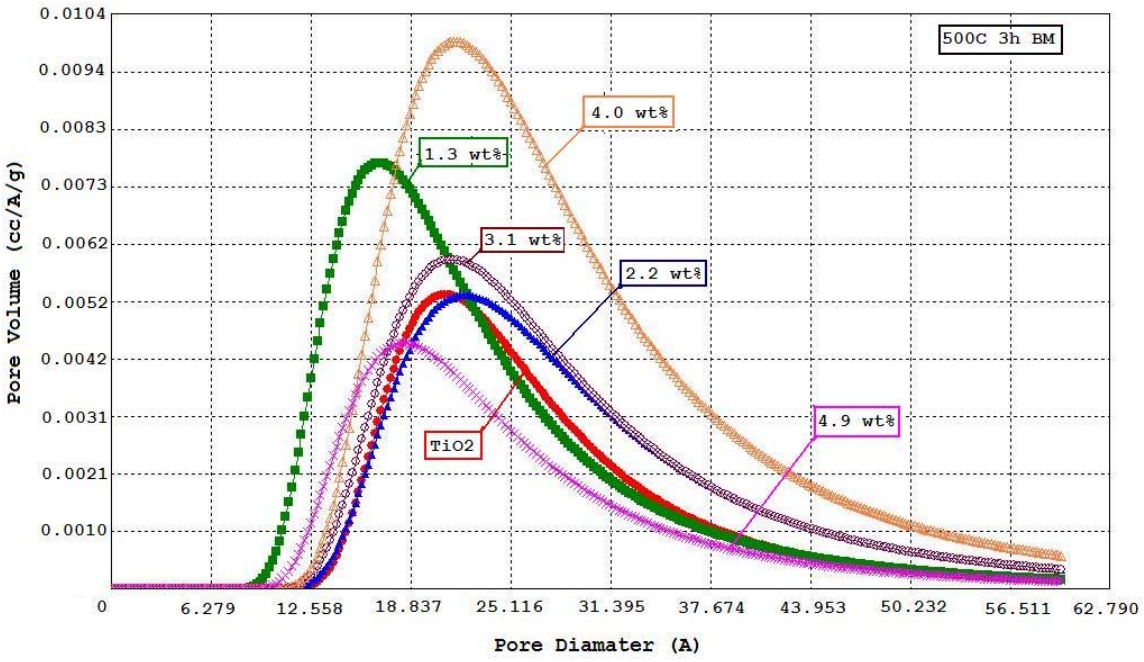

Figure 49 Pore Volume vs Pore Diameter of Zn Doped TiO_2 Annealed After Ball Mill at 500°C 3h

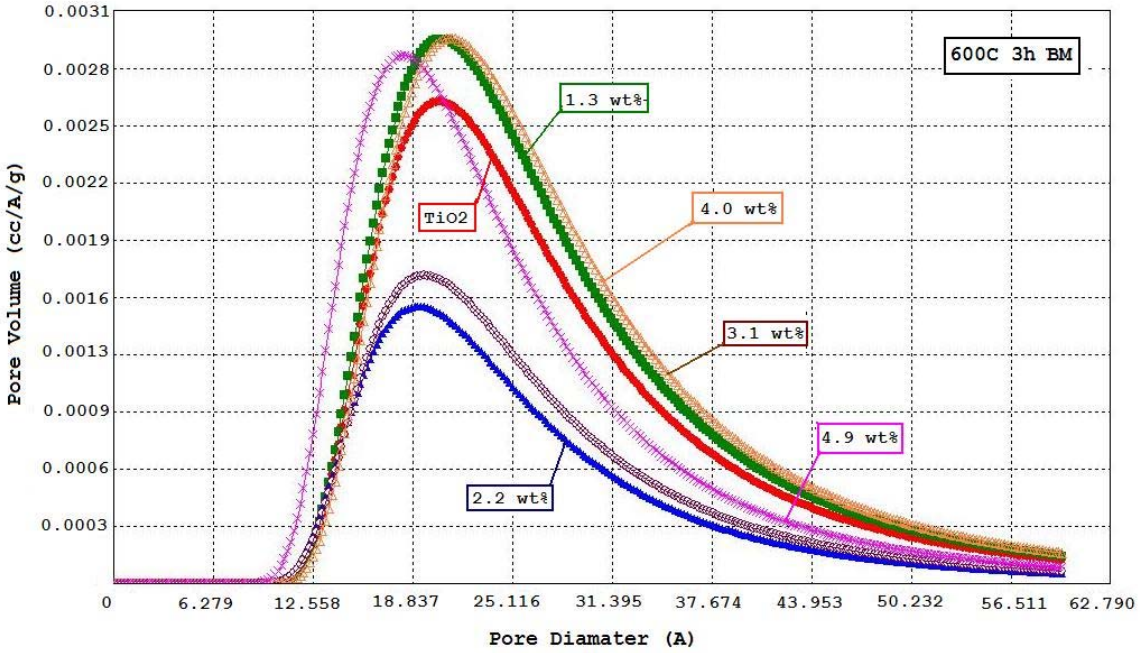

Figure 50. Pore Volume vs Pore Diameter of Zn Doped TiO_2 Annealed After Ball Mill at 600°C 3h

In addition, we can see that the optical absorption measurements of samples prepared by annealing at 500C do not present any variation in the bandgap with the increase of Zn dopant concentration (see Figure 51). However, for Zn doped TiO_2 annealed at 600C, the highest red shift in the band gap of the doped material is observed for 3.1 wt.% Zn doping concentration, which can be seen in Figure 52. Again, such a difference in the effect of the annealing temperature can be explained by the presence of the rutile phase in the samples annealed at 600C (compare Figures 48 and 49). By comparing the optical absorption spectra in Figures. 35 and 51 and Figures. 36 and 52, we can see a blue shift as high as 0.1 – 0.15 eV in the optical absorption, which may be explained by the presence of the quantum size effect.

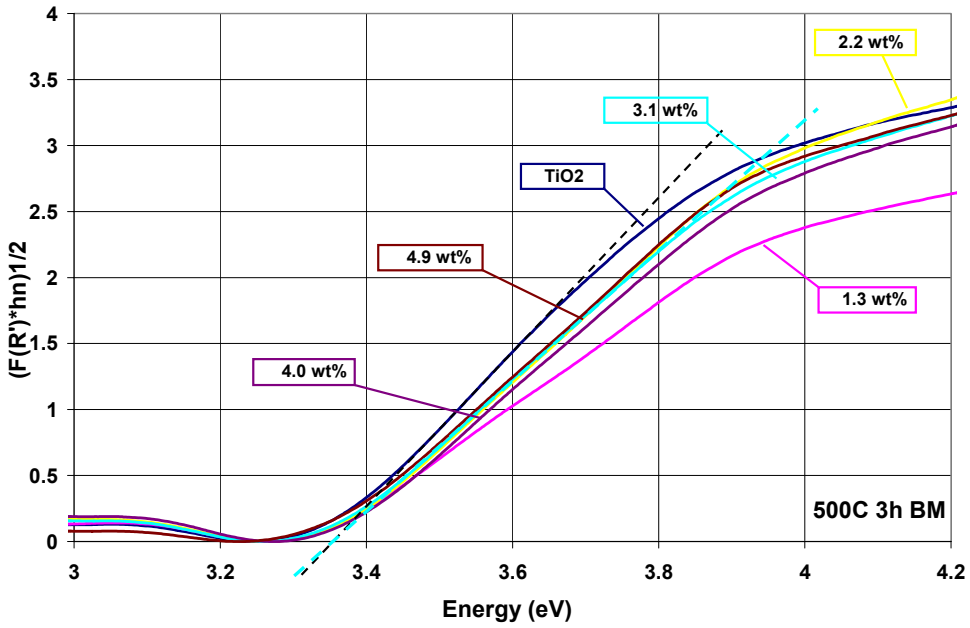

Figure 51 Plot of Optical Absorption (F(R')*hυ)1/2 vs Incident Photon Energy, hυ, for the Sol Gel Samples Annealed at 500C. and Ball Milled for 2 h.

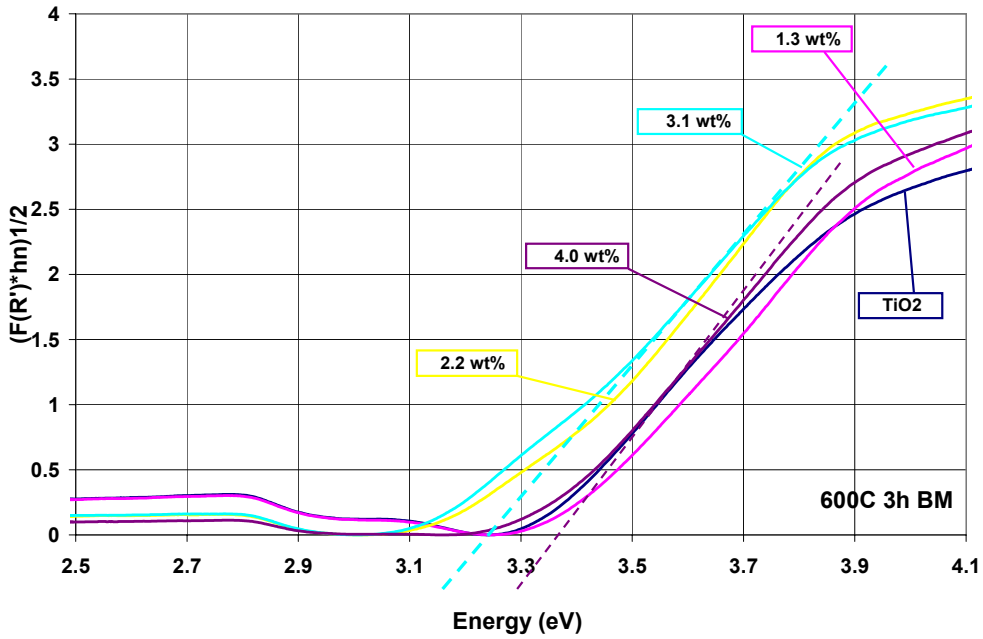

Figure 52. Plot of Optical Absorption (F(R')*hυ)1/2 vs Incident Photon Energy, hυ, for the Sol Gel Samples Annealed at 600C.and Ball Milled for 2h

Finally, the SEM microstructural investigations reveal the variation in the surface morphology with different Zn doping concentrations in the TiO2-Xwt.% Zn nanoparticulates (Figs. 53-65). EDS spectra of these samples confirm the stoichiometric concentration of Zn. Images of SEM are shown in the Figures. 66 and 67.

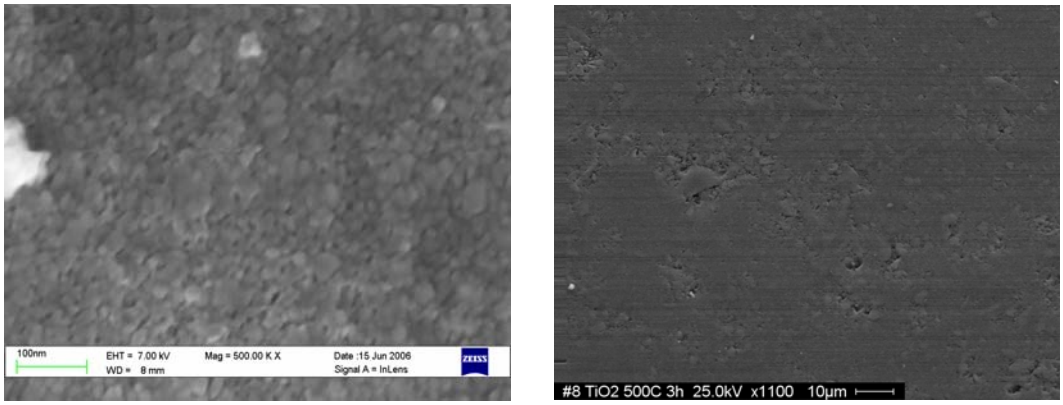

Figure 53. SEM Image of TiO_2 Annealed 500C 3h Before and After Ball Mill.

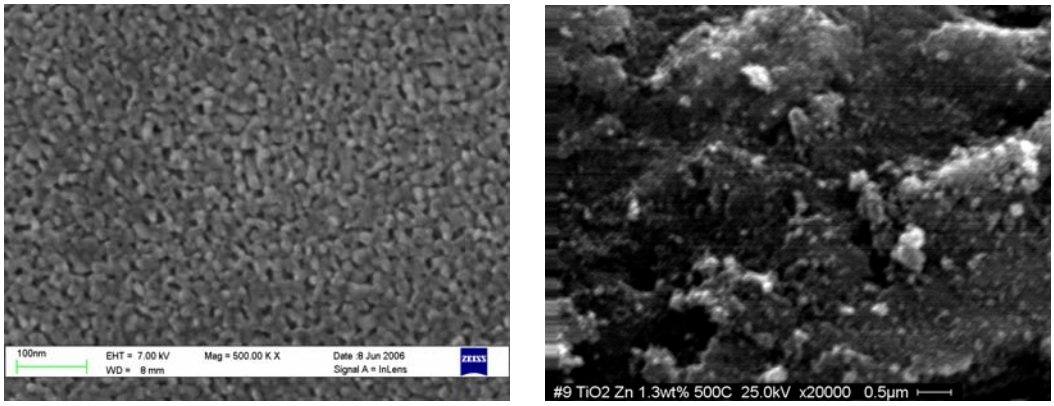

Figure 54 SEM Image of TiO2 Zn Doped at 1.3 wt% 500C 3h Before and After Ball Mill.

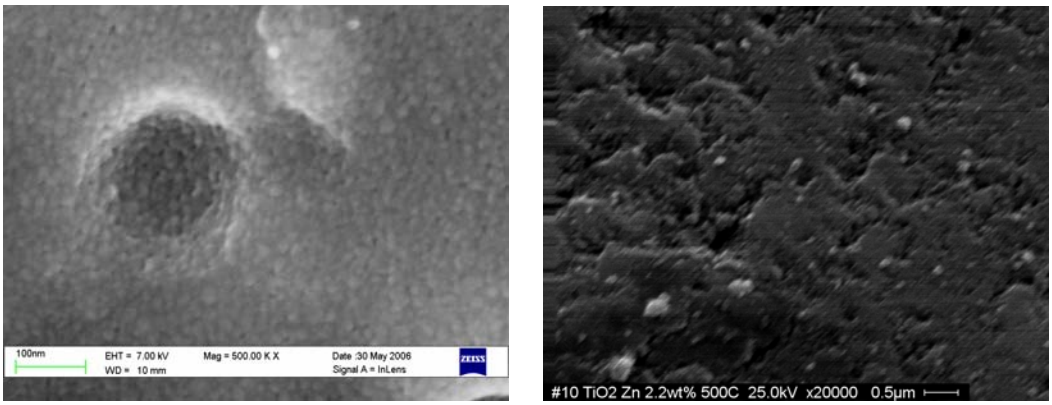

Figure 55 SEM Image of TiO2 Zn Doped at 2.2 wt% 500C 3h Before and After Ball Mill

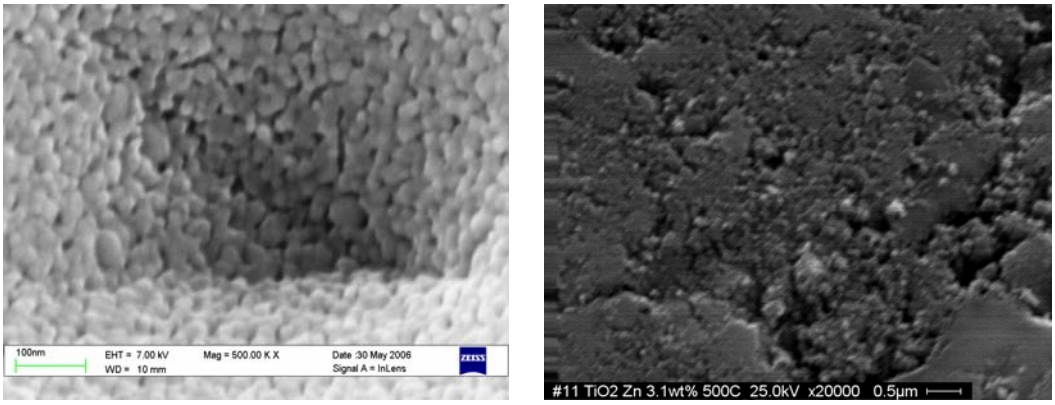

Figure 56 SEM Image of TiO2 Zn Doped at 3.1 wt% 500C 3h Before and After Ball Mill

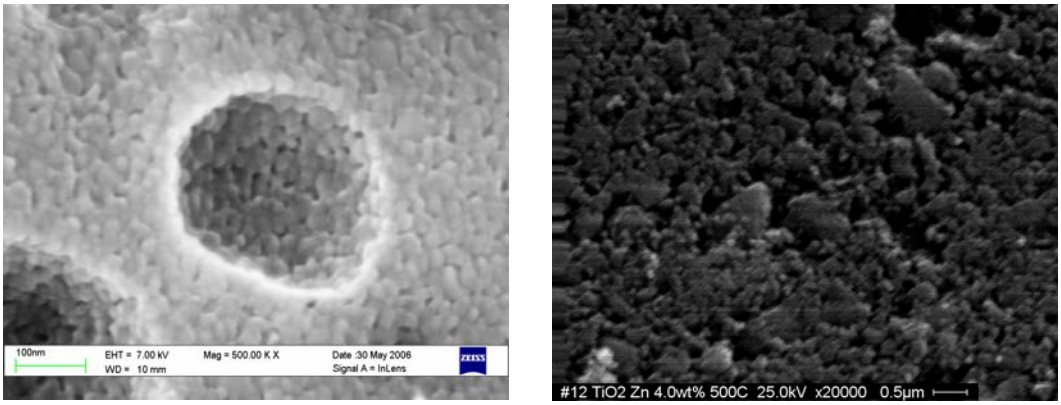

Figure 571 SEM Image of TiO2 Zn Doped at 4.0 wt% 500C 3h Before and After Ball Mill

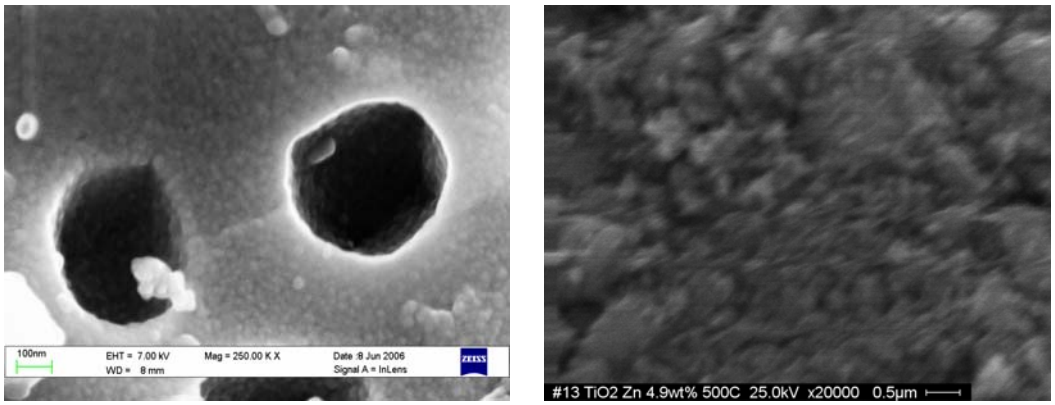

Figure 58 SEM Image of TiO2 Zn Doped at 4.9 wt% 500C 3h Before and After Ball Mill

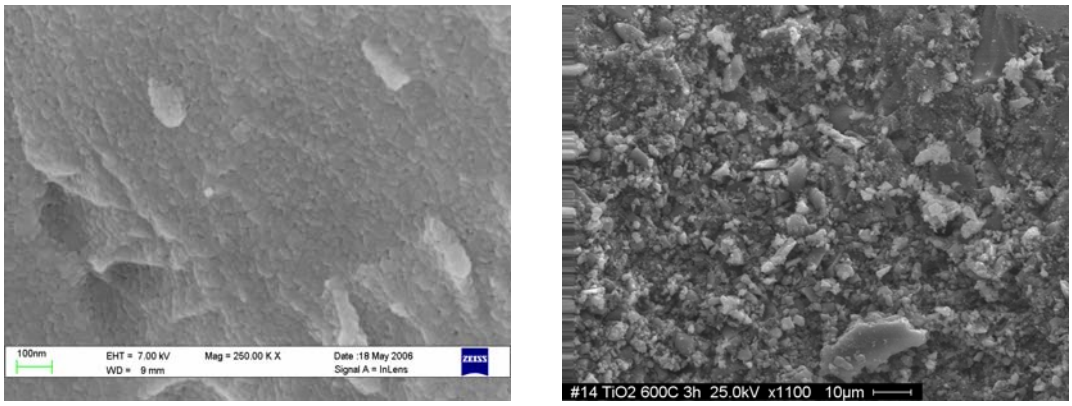

Figure 59 SEM Image of TiO2 Annealed 600C 3h Before and After Ball Mill

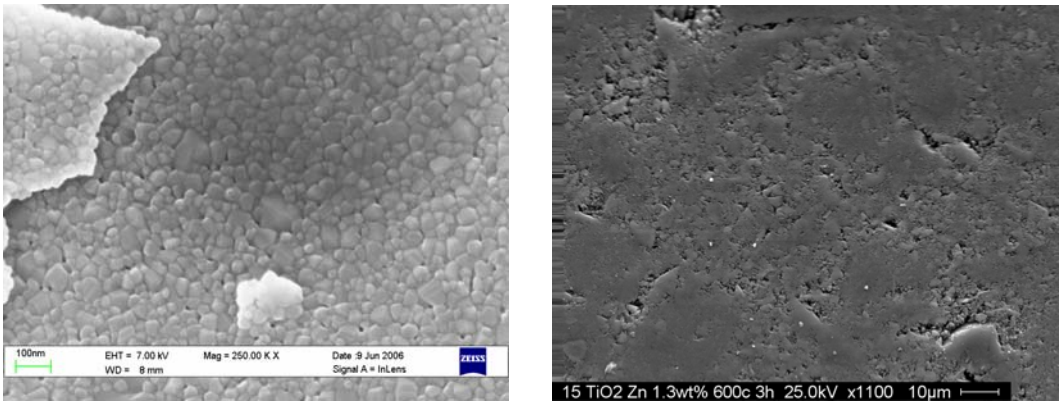

Figure 60 SEM Image of TiO2 Zn Doped at 1.3 wt% 600C 3h Before and After Ball Mill

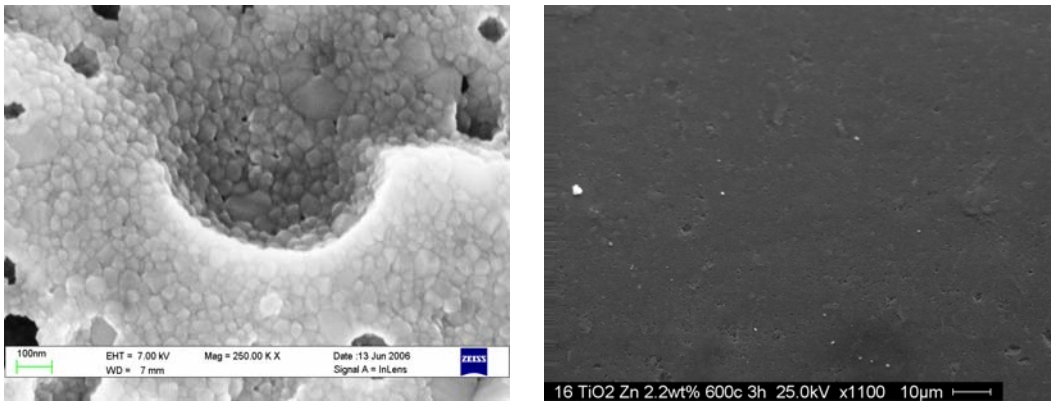

Figure 61. SEM Image of TiO2 Zn Doped at 2.2 wt% 600C 3h Before and After Ball Mill

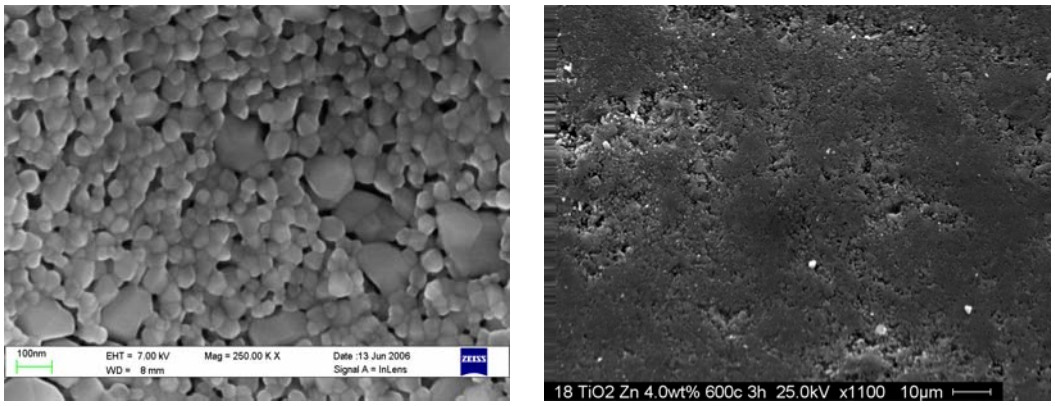

Figure 62. SEM Image of TiO2 Zn Doped at 3.1 wt% 600C 3h Before and After Ball Mill

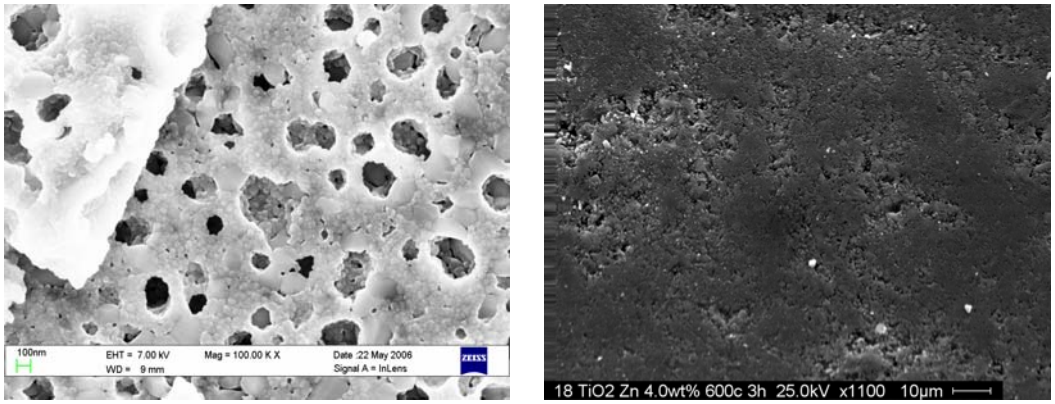

Figure 63. SEM Image of TiO2 Zn Doped at 4.0 wt% 600C 3h Before and After Ball Mill

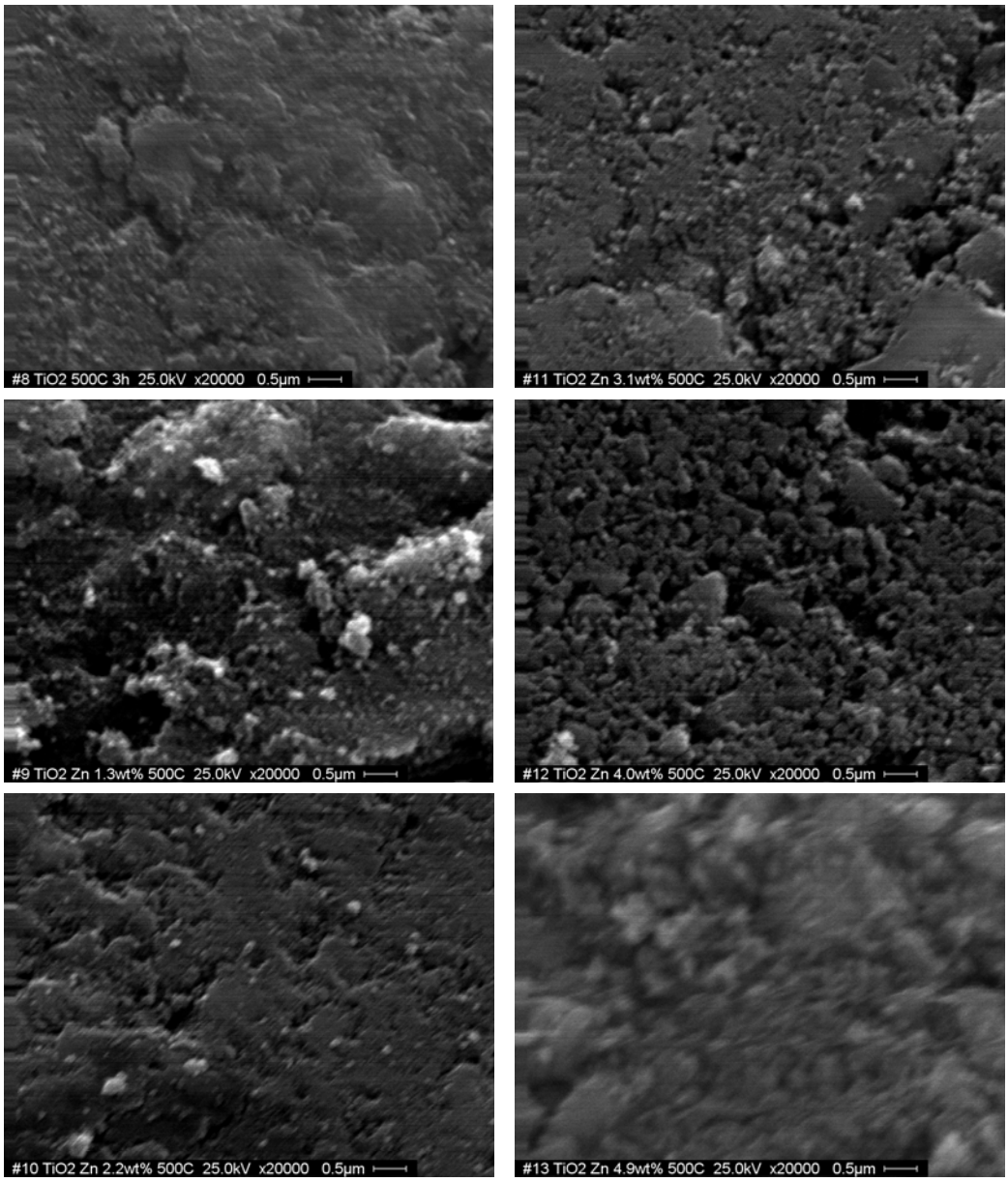

Figure 64. SEM Image ofTiO2 Zn Doped at 500C 3h After Ball Mill at 20000X. Starting Left: 0wt%, 1.3wt%, 2.2 wt%, 3.1 wt%, 4.0 wt% and 4.9 wt%

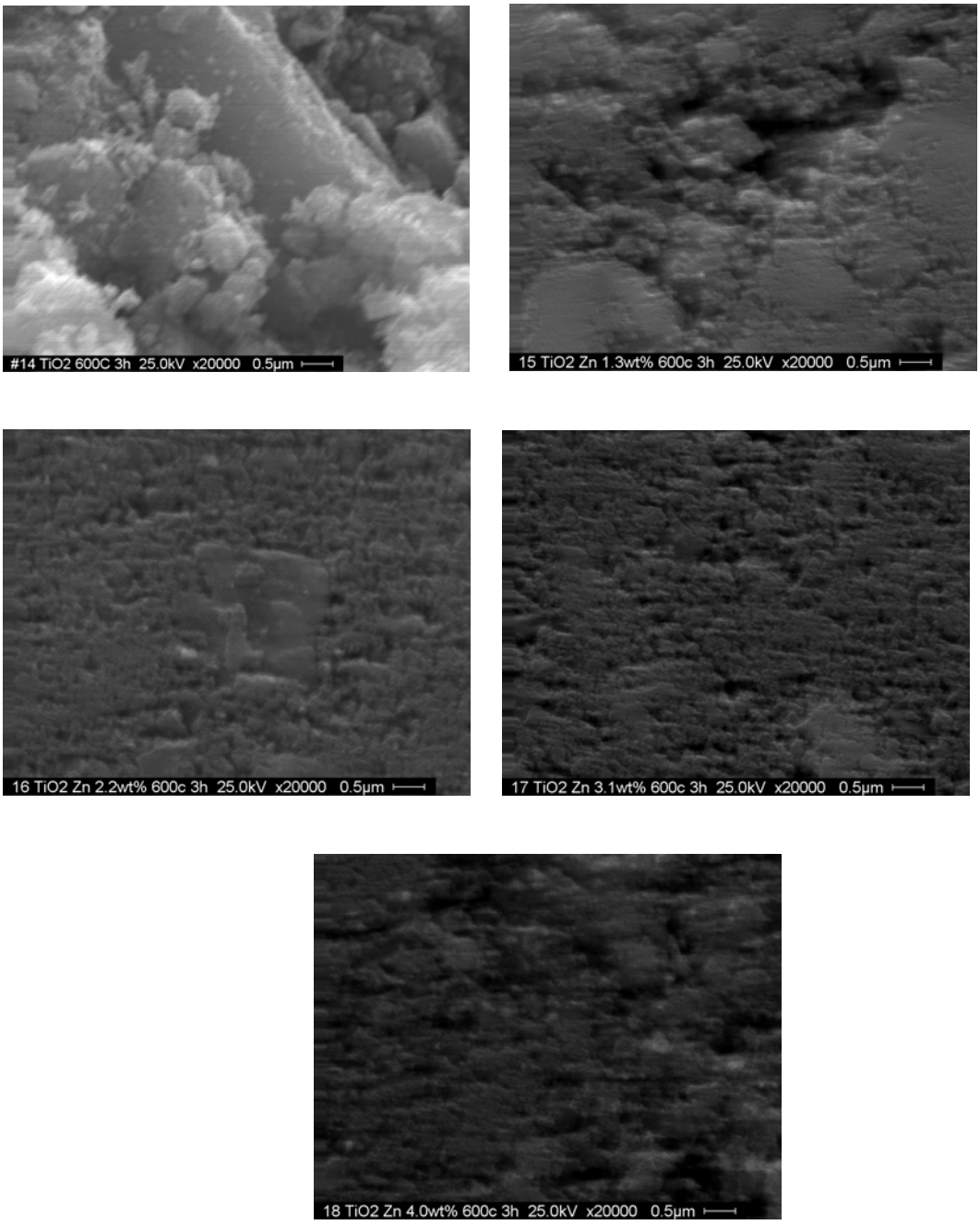

Figure 65. SEM Image ofTiO2 Zn Doped at 600C 3h After Ball Mill at 20000X. Starting Left: 0wt%, 1.3wt%, 2.2 wt%, 3.1 wt% and 4.0 wt%

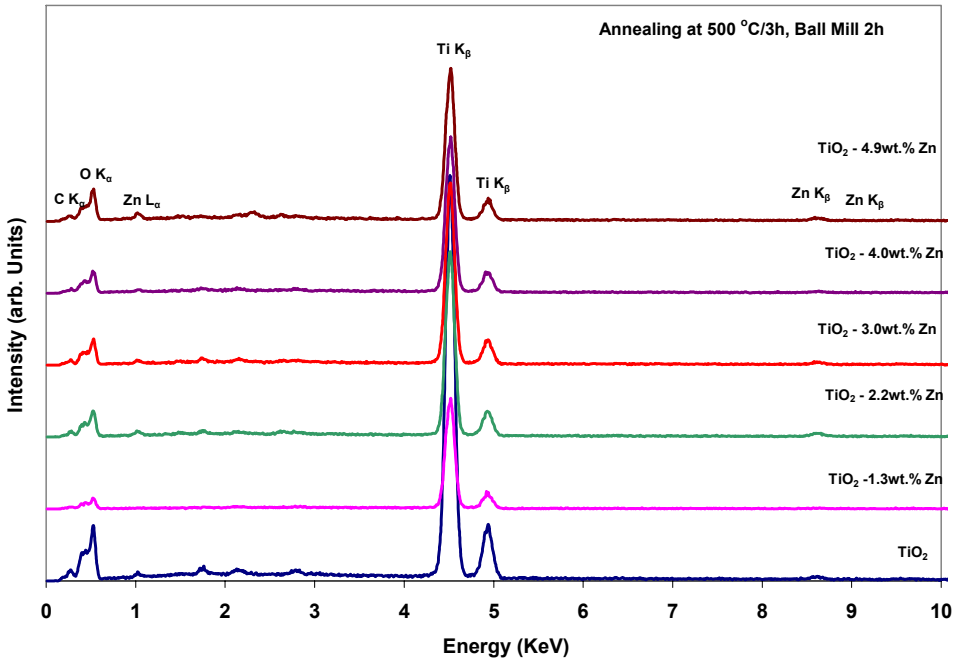

Figure 66. EDS Spectra for 500C 3h Zn Doped TiO2 After Ball Milling

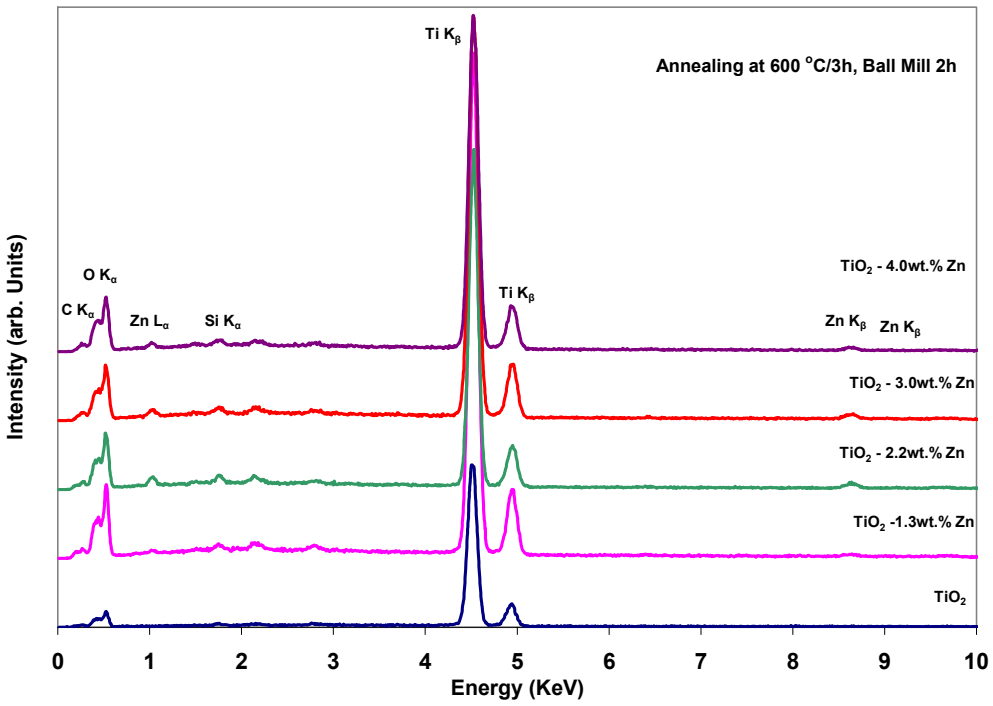

Figure 67. EDS Spectra for 600C 3h Zn Doped TiO2 After Ball Milling

Table 2. EDS values for TiO2 Xwt% Zn 500C After Ball Milling

Sample # (Theorical wt%)		1100X		20000X	
	Element	Wt%	At%	Wt%	At%
8 (0wt%)	OK	35.97	62.71	33.64	60.49
	TiK	64.03	37.29	64.19	38.55
9 (1.3 wt%)	OK	29.11	55.33	31.68	58.27
	TiK	68.9	43.74	66.91	41.1
	ZnK	1.99	0.92	1.41	0.63
10 (2.2 wt%)	OK	35.69	62.8	33.95	61.07
	TiK	60.51	1.64	4.77	2.1
	ZnK	3.8	35.56	61.28	36.83
11 (3.1 wt%)	OK	35.1	62.11	34.9	61.9
	TiK	61.91	36.59	2.98	1.3
	ZnK	2.99	1.29	62.12	36.8
12 (4.0 wt%)	CK	5.17	11.4	5.11	11.3
	OK	33.08	54.75	32.86	0.95
	ZnK	2.03	0.82	2.34	33.14
	TiK	59.73	33.02	59.7	54.61
13 (4.9 wt%)	CK	6.53	13.35	5.36	10.66
	OK	38.34	58.87	42.77	63.86
	ZnK	3.54	26.46	2.9	24.42
	TiK	51.59	1.33	48.97	1.06

Table 3. EDS values for TiO2 Xwt% Zn 500C After Ball Milling

Sample (Theorical Zn wt%)		1100X		20000X	
	Element	Wt%	At%	Wt%	At%
14 (0wt%)	OK	28.98	54.99	28.91	54.9
	TiK	71.02	45.01	71.09	45.1
15 (1.3 wt%)	OK	34.62	61.42	32.7	59.39
	TiK	64.34	38.13	66.03	40.05
	ZnK	1.04	0.45	1.26	0.56
16 (2.2 wt%)	OK	40.28	67.03	-	-
	SiK	0.64	0.6	36.84	63.91
	TiK	55.92	31.08	59.86	34.69
	ZnK	3.17	1.29	3.3	1.4
17 (3.1 wt%)	OK	35.36	62.19	32.54	59.2
	SiK	0.65	0.66	0.71	0.74
	TiK	61.21	35.95	63.69	38.7
	ZnK	2.78	1.19	3.06	1.36
18 (4.0 wt%)	TiL	26.47	16.6	27.44	17.4
	OK	30.25	56.79	29.34	55.72
	ZnL	1.79	0.82	1.85	0.86
	TiK	40.13	25.16	40.07	25.42
	ZnK	1.36	0.62	1.3	0.6

Comparing Figures 46 and 51 one can see that Zn concentration of 1.3 wt % is an optimum for obtaining higher photocatalytic efficiency for the ball milled TiO2-Xwt.% Zn samples calcinated at 500°C with an optimum pore volume size. The correlation between the increase of photocatalytic activity and the BET surface area implies that the liquid-solid interface of ball- milled samples plays an important role in the improvement of the photocatalytic activity for the Zn doped TiO_2. For the samples calcinated at 600°C, the maximum photocatalytic activity was observed for the samples with 4.9 wt.% Zn doping.

Thus we can conclude that the proposed new strategy to reduce the average crystallite size and optimize the micropore size distribution by mechano-chemically milling TiO2-Xwt.% Zn in a high energy planetary mill has resulted in average improvement of the photocatalytic activity by a two fold increase as it can be seen in Figures 42 and 43.

CHAPTER 8: SUMMARY AND CONCLUSIONS

The Results of this study are as follows:

1. Attempts were made to improve the photocatalytic behavior of TiO2 by doping with various concentrations of Zn (0, 1.3, 2.2, 3.1, 4.0 and 4.9) in a sol-gel process.

2. There is no significant change in the photocatalytic efficiency for TiO2-Xwt.% Zn processed at two different calcination temperatures (500 and 600 °C).

3. The reason for this may be due to the large crystallite sizes and the lower surface area of these initial samples observed from XRD and BET analysis.

4. Pursued a new strategy to reduce the average crystallite size and optimize the micropore size distribution by mechano-chemically milling TiO2-Xwt.% Zn in high energy planetary mill.

5. This approach resulted in average improvement of the photocatalytic activity by a two fold increase which can be explained by: a) increase in the surface area by two times and b) decrease in average cyrstallite size by two times.

6. Zn concentration of 1.3 wt.% is optimum for obtaining higher photocatalytic efficiency for the ball milled TiO2-Xwt.% Zn samples calcined at 500°C.

7. For the case of samples calcined at 600°C, the maximum photocatalytic behavior was observed for TiO2 - 4.9 wt.% Zn.

8. The above photocatalytic enhancement of TiO2-Xwt.% Zn can be explained by the increase in the surface area and the optimized size of the particles.

9. Comparing the Kubelka-Munk spectra of pristine and ball milled samples revealed a blue shift (increase in Eg) from 3.2 eV to 3.35 eV, which may be because of the presence of quantum size effects.

10. SEM microstructural investigations revealed variations in the surface morphology with different Zn doping concentrations in the TiO2-Xwt.% Zn nanoparticulates. EDS spectra of these samples confirmed the stoichiometric concentration of Zn.

Experimental observations also suggest that the average crystallite size measurements obtained from the XRD analysis and BET surface area calculations are in good agreement with each other.

LIST OF REFERENCES

[1] S. Malato, J. Blanco, D. Alarco´n, M. Maldonado, P. Fernández-Ibáñez, W. Gernjak, “Photocatalytic decontamination and disinfection of water with solar collectors,” *Catalysis Today* vol. 122, pp.137–149, 2007

[2] M. Kositzi, I. Poulios, S. Malato, J. Caceres, A. Campos, "Solar photocatalytic treatment of synthetic municipal wastewater," *Water Research,* vol. 38, pp. 1147-1154, 2004

[3] A. Fujishima, X. Zhang, "Titanium dioxide photocatalysis: present situation and future approaches," *C.R. Chimie,* vol. 9, pp. 750-760, 2006

[4] O. Carp, C. L. Huisman, and A. Reller, "Photoinduced reactivity of titanium dioxide," *Progress in Solid State Chemistry,* vol. 32, pp. 33-177, 2004

[5] K. Madhusudan Reddy, B. Baruwati, M. Jayalakshmi, M. Mohan Rao, and S. V. Manorama, "S-, N- and C-doped titanium dioxide nanoparticles: Synthesis, characterization and redox charge transfer study," *Journal of Solid State Chemistry,* vol. 178, pp. 3352-3358, 2005

[6] M. Schmidt, " Thermochemical Treatment of TiO_2 Nanoparticles for Photocatalytic Applications,"*University of South Florida,* 2007

[7] N. A. Serpone, Emeline, A.V., "Suggested terms and definitions in photocatalysis and radiocatalysis," *International Journal of Photoenergy,* vol. 4, pp. 91-131, 2002

[8] T. Ohno, K. Sarukawa, K. Tokieda, and M. Matsumura, "Morphology of a TiO_2 Photocatalyst (Degussa, P-25) Consisting of Anatase and Rutile Crystalline Phases," *Journal of Catalysis,* vol. 203, pp. 82-86, 2001

[9] M. Schiavello, *Heterogeneous Photocatalysis, Volume 3,* First ed. Baffins Lane, Chichester: Wiley, 1997

[10] A. Sobczynski, A. Dobosz, "Water Purification by Photocatalysis on Semiconductors," *Polish Journal of Environmental Studies,* vol. 10, pp. 195-205, 2001

[11] U. Diebold, "The surface science of Titanium dioxide," *Surface Science Reports,* vol. 48, pp. 53-229, 2003

[12] A. Mills, R. Davies, D. Worsley, "Water Purification by Semiconductor Photocatalysis," *Chemical Society Reviews,* vol. 22, pp.417-425, 1993

[13] Y. Paz, Z. Luo, L. Rabenberg, A. Heller, "Photooxidative self-cleaning transparent titanium dioxide films on glass," *Journal of Materials Research,* vol. 10, pp. 2842, 1995

[14] A. K. Datye, G. Riegel, J. R. Bolton, M. Huang, and M. R. Prairie, "Microstructural Characterization of a Fumed Titanium Dioxide Photocatalyst," *Journal of Solid State Chemistry,* vol. 115, pp. 236-239, 1995

[15] S. Al-Qaradawi, S. R. Salman, "Photocatalytic degradation of methyl orange as a model compound,"*Journal of Photochemistry and Photobiology A: Chemistry,* vol. 148, pp. 161-168, 2002

[16] A. L. Linsebigler, G. Lu, and J. T. Yates, "Photocatalysis on TiO_2 Surfaces: Principles, Mechanisms, and Selected Results," *Chemical Reviews*. vol. 95, pp. 735-758, 1995

[17] D. Hufschmidt, L. Liu, V. Selzer and D. Bahnemann, "Photocatalytic water treatment: fundamental knowledgerequired for its practical application," *Water Science and Technology,* vol. 49, pp. 135–140, 2004

[18] I. A. Shkrob and M.C. Sauer, "Hole Scavenging and Photo-Stimulated Recombination of Electron-Hole Pairs in Aqueous TiO2 Nanoparticles," *Journal of Physics and Chemistry,* vol. 108, pp. 12497-12511, 2004

[19] D. Bahnemann, “Photocatalytic water treatment: solar energy applications," *Solar Energy,* vol. 77, pp. 445–459, 2004

[20] S. Rodrıguez, J. Blanco, M. Fernandez, D. Alarcon, M. Collares, J. Farinha, “Engineering of solar photocatalytic collectors,” *Solar Energy*, vol. 77, pp. 513-524, 2004

[21] T.Ohno, K. Sarukawa and M. Matsumura, "Crystal faces of rutile and anatase TiO2 particles and their rolesin photocatalytic reactions," *The Royal Society of Chemistry and the Centre National de la Recherche Scientifique*, vol. 26, pp. 1167-1170, 2002

[22] A. Tsujiko, T. Kisumi, Y. Magari, K. Murakoshi and Y. Nakato, " Selective Formation of Nanoholes with (100)-Face Walls by Photoetching of *n*-TiO2 (Rutile) Electrodes, Accompanied by Increases in Water-Oxidation Photocurrent," *Journal Physics and Chemistry. B*, vol. 104, pp. 4873-4879, 2000

[23] T. Sugiura, S. Itoh, T. Ooi, T. Yoshida, K. Kuroda and H. Minoura," Evolution of a skeleton structured TiO2 surface consisting of grain boundaries," *J. Electroanal. Chem.*, vol. 473, pp. 204-208, 1999

[24] W. C. Hao, S. K. Zheng, C. Wang, "Comparison of the photocatalytic activity of TiO2 powder with different particle size," *Journal of Materials Science Letters*. vol. 21, 1627-1629, 2002

[25] L. Jing, B. Xin, F. Yuan, L. Xue, B. Wang, and H. Fu, "Effects of Surface Oxygen Vacancies on Photophysical and Photochemical Processes of Zn-Doped TiO2 Nanoparticles and Their Relationships," *J. Phys. Chem. B,* vol. 110, pp. 17860-17865, 2006

[26] W. Zhanga, S. Zhub, Y. Lib, F. Wang, "Photocatalytic Zn-doped TiO2 films prepared by DC reactive magnetron sputtering," *Vacuum,* vol. 82, pp. 328–335, 2008

[27] N. Guettai and H. Ait Amar, "Photocatalytic oxidation of methyl orange in presence of titanium dioxide in aqueous suspension. Part I: Parametric study," *Desalination,* vol. 185, pp. 427-437, 2005

[28] K.T. Chung, G.E. Fulk and A.W. Andres, "Mutagenicity testing of some commonly used dyes," *Applied and Environmental Microbiology*, vol. 42, pp. 641–648, 1981

[29] S. Doh, C. Kim, S. G. Lee, S. J. Lee, H Kim, "Development of photocatalytic TiO2 nanofibers by electrospinning and its application to degradation of dye pollutants," *Journal of Hazardous Materials*, 2007

[30] A.R. Phani, "Structural evolution and its effect on photocatalytic properties of pure TiO_2 and Zn doped TiO_2 nanopowders," *NANO-Center for Advanced Nanotechnologies Presentation,* Nov. 2007

[31] M.N. Rashed, A.A. El-Amin, “Photocatalytic degradation of methyl orange in aqueous TiO2 under different solar irradiation sources,” International Journal of Physical Science, vol. 2, pp. 73-81, 2007

[32] Y. Zhao, C. Li, X. Liu, F. Gu, H.L. Du, L Shi, "Zn-doped TiO2 nanoparticles with high photocatalytic activity synthesized by hydrogen-oxygen diffusion flame," *Applied Catalysis B: Environmental,* vol. 79, pp. 208–215, 2008

[33] G. Marcı, V. Augugliaro, M. Lopez-Munoz, C. Martın, L. Palmisano, V. Rives, M. Schiavello, R. J.Tilley, A. Venezia, "Preparation Characterization and Photocatalytic Activity of Polycrystalline ZnO/TiO2 Systems. 2. Surface, Bulk Characterization, and 4-Nitrophenol Photodegradation in Liquid-Solid Regime," *J. Phys. Chem. B,* vol. 105, pp. 1033-1040, 2001

[34] D. Escobar, " Investigation of ZrNi, $ZrMn_2$ and $Zn(BH_4)_2$ Metal/Complex Hydrides for Hydrogen Storage," *University of South Florida,* 2007

[35] NNRC, Training Material for X-Ray Diffraction, *University of South Florida*, 2007

[36] On line post: http://www.quantachrome.com/gassorption/index.html

[37] New Mexico tech. “FESEM types of signals,” online posting, http://infohost.nmt.edu/~maximino/fesem_types_of_signals.htm.

[38] ETH Zürich website. “SEM technology,” online posting, www.microscopy.ethz.ch/sem.htm.

[39] N. Venkatachalam, M. Palanichamy, V. Murugesan, "Sol–gel preparation and characterization of nanosize TiO2: Its photocatalytic performance," *Materials Chemistry and Physics*, vol. 104, pp. 454–459, 2007

[40] D. Di Claudio, A.R. Phani, S. Santucci, "Enhanced optical properties of sol–gel derived TiO2 films using microwave irradiation," *Optical Materials*, vol. 30, pp. 279–284, 2007

[41] A.R. Phani, "Structural evolution and its effect on photocatalytic properties structural evolution and its effect on photocatalytic properties of of pure TiO pure TiO2 and Zn doped TiO and Zn doped TiO2 nanopowders," *Department of Physics, University of L’Aquila*, Nov. 2007

[42] Quantachrome Instrument, Autosorb 1, Operation Manual, pp 68-70, 2005

[43] P.G. McCormick, F.H. Froes, "The Fundamentals of Mechanochemical Processing,"*JOM*, pp. 61- 65, 1998

[44] The Glassware Gallery. “Planetary ball milling,” online posting, www.ilpi.com/inorganic/glassware/ballmill.html.

[45] C. Wu, L. Feng, Y. Kuo, C. Shu, "Enhancement of the photocatalytic activity of TiO2 film via surface modification of the substrate," *Applied Catalysis A,* vol. 226, pp. 199-211, 2002

[46] S. Jane, S Cheng, "Effect of TiO: crystalline structure in photocatalytic degradation of phenolic contaminants," vol. 33, pp. 227-237, 1997

[47] S. Darrin, J L. Falconer,"Catalyst Design to Change Selectivity of Photocatalytic Oxidation," *Journal of Catalysis,* vol.175, pp 213-219, 1998

[48] Online posting:http://www.rpi.edu/dept/phys/ScIT/InformationProcessing